

Optimization and comparison of multiple solar energy systems for public sanitation service buildings in Tibet

Yaowen Chen ^{a,b,*}, Mengchen Quan ^b, Dengjia Wang ^{a,b}, Hu Du ^{c,d}, Liang Hu ^b, Yiting Zhao ^b, Mengmeng Guo ^b, Yanfeng Liu ^{a,b}

^a State Key Laboratory of Green Building in Western China, Xi'an University of Architecture and Technology, No. 13 Yanta Road, Xi'an 710055, China ^b School of Building Services Science and Engineering, Xi'an University of Architecture and Technology, No. 13 Yanta Road, Xi'an 710055, China ^c Welsh School of Architecture, Cardiff University, Bute Building, King Edward VII Avenue, Cardiff CF10 3NB, UK ^d School of Civil Engineering and Built Environment, Liverpool John Moores University, Cherie Booth Building, Byrom St, Liverpool L3 3AF, UK

Abstract

Qinghai Tibet Plateau, known as 'Roof of the World', is the highest and largest plateau on Earth, with an average elevation of 4900 m and spanning nearly two-thirds the size of the European continent. The energy consumption characteristics of public sanitation service buildings in the Qinghai Tibet Plateau are significantly different from traditional public buildings. It has unique advantages that allow these facilities to use the local enriched solar energy resources to meet the energy demand. This study proposes eight potential solar energy system schemes to obtain a suitable solar energy supply system and design an optimization method for public sanitation service buildings. The optimization models aimed at the life cycle cost for each solar energy system are established, and the equipment capacity in the system is optimized and simulated. Firstly, the optimized life cycle cost and equipment capacity of different solar energy system are compared and analyzed. Then, the short-term dynamic operation performance and the system's energy conservation, economic and CO₂ emission reduction performance are comprehensively analyzed. Finally, the sensitivities of economic parameters and equipment price to the system optimization results are analyzed. The results indicate that the life cycle cost of the integrated solar hot water and heat storage system is 43% lower than that of the standalone solar hot air heat supply system and the standalone photovoltaic system. An optimized integrated system consisting of photovoltaic, photothermal, thermal storage, and power storage has the best comprehensive performance. The annual energy saving ratio of the integrated system is ~85%, and the life cycle cost saving rate is about 50%. In addition, the sensitivity analysis shows that the electricity price is the most significant factor for life cycle cost compared to the annual interest and inflation rates. The price of a solar collector and air source heat pump have the most significant impact on the life cycle cost optimization results of a photovoltaic-photothermal-thermal and power storage integrated system.

1. Introduction

Tourists worldwide visit the Qinghai Tibet Plateau (with an average elevation of 4900 m) to partake in the unique natural scenery and regional folk culture. In recent years, with increasing transportation facilities on the Qinghai Tibet Plateau, local tourism has rapidly increased. Through 2018, the total number of tourists exceeded 120 million [1]. While the development of tourism drives local economic development, it also requires enhanced public infrastructure service for

cities and the surrounding scenic locations. Public sanitation service buildings (PSSBs) are essential public service facilities and vital benchmarks measuring the quality of the tourism service industry. Therefore, it is vital to increase the service level of PSSBs for improving the satisfaction of tourists and the quality of life of the surrounding residents.

Limited by the economic conditions of the Qinghai Tibet Plateau, the development of local PSSBs has lagged. The singularity of the functions of the local traditional public toilets has several defects, such as unpleasant indoor odors, poor sanitary conditions, and low temperature in the winter, and has been unable to meet the needs of residents and tourists. In 2016, the "Toilet Revolution" policy was comprehensively promoted, and higher requirements were implemented for the service level of public toilets in the Qinghai-Tibet Plateau. In 2017, the local government prepared the "Technical guidelines for the revolution of public toilets in the Tibet Autonomous Region" to guide public toilet construction, operation, and maintenance in urban and rural areas and scenic spots [2]. With implementing a series of policies, the traditional public toilets gradually progress towards multi-function, comfortable, and healthier PSSBs (Fig. 1).

Nomenclature a_1 First order efficiency coefficient of heat

collection efficiency

a_2 Second order efficiency coefficient of heat collection efficiency

A_{SC} Effective heat collection area of the solar collector, m^2

A_T Surface area of the water tank in contact with the environment, m^2

A_{PV} PV area, m^2

A_{SC} Solar collector area, m^2 A_{max} Maximum installation area of roof,

m^2 c_p Constant pressure specific heat capacity of water, $kJ \cdot kg^{-1} \cdot K^{-1}$

C_{Bat} Rated power of the battery, CNY

C_{IN} Initial investment of the system, CNY

C_{RE} Replacement cost, CNY

C_{OM} Operation and maintenance cost, CNY

C_{SV} System salvage value, CNY d Annual

interest rate

E_{PV} Electricity generation of PV system, kWh

E_{Grid} Electricity provided by municipal power grid, kWh

E_{BE} Electricity consumption of the basic equipment, kWh

E_{PE} Electricity consumption of the power equipment, kWh

E_{ASHP} Electricity consumption of the air source heat pump, kWh

E_{EH} Electricity consumption of electrical heater, kWh

E_{LOSS} Electricity loss, kWh

P_c Battery charging power, kW

P_d Battery discharging power, kW

E_{Bat} Remaining electric energy in the battery, kWh

$P_{Bat,max}$ Maximum rated power of battery, W

E_{con} Annual electricity consumption of the contrast system, kWh

E_{SS} Annual electricity consumption of the different solar energy supply system, kWh

f_{PV} PV derating factor f

Annual inflation rate

Q_{EH} Heat supply of the electric heater, GJ

G_T Total tilted surface radiation of the solar collector, $W \cdot m^{-2}$

LCC_{con} Life cycle cost of the contrast system, CNY LCC_{SS}

Life cycle cost of the solar energy supply system, CNY $L_{CO_2,con}$

Operation CO_2 emission of the contrast system, m^3

$L_{CO_2,SS}$ Operation CO_2 emission of the solar energy supply system, m^3 .

m_{ST} Flow rate of solar heat collection system, $kg \cdot h^{-1}$ m_{HL}

Flow rate of heating system, $kg \cdot h^{-1}$ m_{WL} Flow rate of hot water system, $kg \cdot h^{-1}$ N System design life cycle, year

Y_{PV} Rated power of PV cells, kW

$V_{Tank,max}$ Maximum heat storage volume of heat storage tank, m^3

V_{Tank} Heat storage tank volume, m^3

U Heat transfer coefficient of water tank, $W \cdot m^{-2} \cdot K^{-1}$

T_i Average water temperature of node i of heat storage tank, $^{\circ}C$

T_{WL} Mains water temperature, $^{\circ}C$ T_{HL}

Return temperature of the heating system, $^{\circ}C$

T_{ST} Outlet temperature of the solar collector, $^{\circ}C$

T_{amb} Ambient temperature, $^{\circ}C$

T_{in} Inlet temperature of collector, $^{\circ}C$ $T_{c,STC}$

PV cell temperature under STC, $^{\circ}C$

T_c PV module instantaneous temperature, $^{\circ}C$ T^*

Normalized temperature difference

S_{ASHP} Control signal of the air source heat pump S_d

Charge and discharge depth of the battery $Q_{Load,max}$ Maximum

hourly heating load of buildings, GJ Q_{LOSS} Heat loss of

system, GJ Q_{TES} Heat stored/released in water tank, GJ

Q_{ASHP} Heat supply of the air source heat pump, GJ

Q_{SC} Heat supply of the solar collector, GJ

C_{Bat} Battery capacity, kWh *Greek symbols* η_c Battery

charging efficiency, % η_d Battery discharging efficiency, %

α_P PV temperature coefficient for the power, $\% \cdot ^{\circ}C^{-1}$ η_{SC}

Solar collector efficiency, % η_0 Solar collector thermal efficiency

at $T^*=0$, % μ Ratio of equipment maintenance cost to

equipment purchase cost

ϕ System salvage value ratio

Abbreviation

PSSBs Public sanitation service buildings

NOCT Normal operating cell temperature SOC

State of charge

COP Coefficient of performance of ASHP

SESS Solar energy supply system LCC

Life cycle cost

LCCSR Life cycle cost saving rate

ACRR Annual carbon reduction rate

SHS Solar heating system

CCHP Combined cooling heating and power system

PSO Particle swarm optimization ASHP

Air source heat pump

SHAS Solar hot air heat supply system

PV Photovoltaic

PT Photothermal

TES Thermal energy storage

EES Electricity energy storage

AEC Annual energy consumption of the system

AESR The annual energy saving ratio

MEP Municipal electricity price PCM

Phase change material

PVT Photovoltaic thermal module EWH

Electric water heater

However, with the addition of multiple functions such to PSSBs as heating, hot water, hand drying, disinfection, and fresh air, these buildings consume more energy. The energy demand of multi-functional PSSBs is primarily centered on heating and electricity. The heat energy is mainly supplied for indoor space heating and hot water. In addition to meeting the consumption of electrical appliances (exhaust fan, mobile phone, lighting, disinfection, deodorization machine, etc.) and power equipment (circulating water pump, fan, etc.), electricity can also be converted into heat through energy conversion equipment (heat pump, electric water heater, etc.). It is critical to

Research on active solar heating systems (SHS) mainly focuses on improving equipment components, system performance evaluation, system optimization design, operation control strategy, etc. Wang et al. [9], Xu et al. [10], Saxena et al. [11], and Palacio et al. [12] have performed experimental and numerical simulation studies on the thermal performance of new solar collectors, including large-size flat plate collectors, nanomagnetic collectors, air collectors, and phase change material (PCM) collectors. Pandey et al. evaluated the thermal performance of SHS based on thermodynamics and determined that the energy efficiency of SHSs varies under different flow

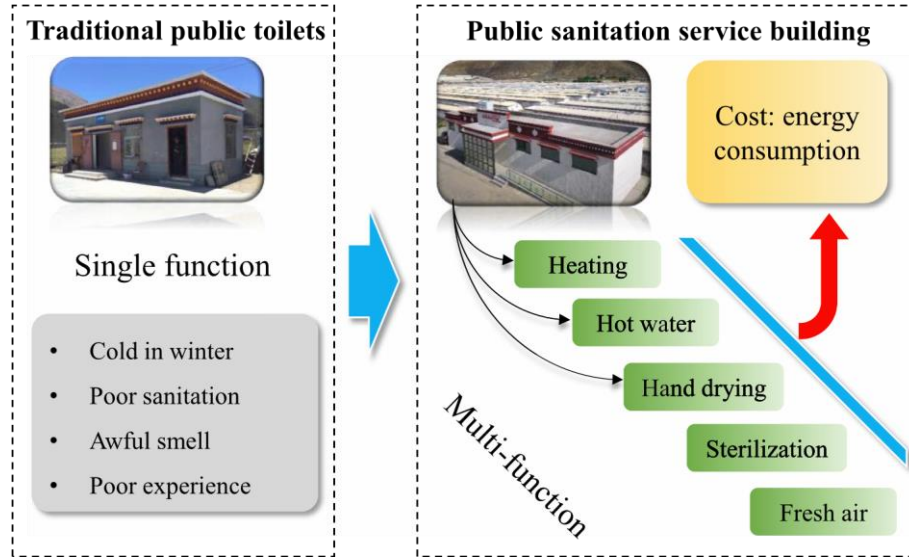


Fig. 1. Comparison between PSSBs and traditional public toilets.

design an appropriate energy supply system for the development and application of PSSBs according to the energy demand.

In the Qinghai-Tibet Plateau, conventional energy is scarce and mainly depends on the import from other regions of China. Consequently, the extensive use of traditional energy will inevitably cause high operation costs and a high risk of ecological environment damage [3]. The energy support system of PSSBs on the Qinghai-Tibet Plateau should focus on finding suitable local renewable energy sources to reduce emissions while ensuring the reliability and economy of the system. It is widely known that the region has low air pressure low and abnormally high local solar energy resources, with the annual solar irradiation exceeding $5400 \text{ MJm}^{-2} \cdot \text{a}^{-1}$ or $1500 \text{ kWhm}^{-2} \cdot \text{a}^{-1}$. These factors suggest that solar energy resources are viable for PSSBs [4]. In addition, almost all local public toilet buildings are low rise buildings with one or two floors, and the ratio of roof area to building area is high. Such buildings have sufficient solar energy collection surfaces, suggesting that solar energy is a good choice for energy generation for PSSBs in the Qinghai-Tibet Plateau.

1.1. Solar heat collection and heating

The utilization of solar energy in buildings is generally divided into two forms, solar photothermal utilization and photoelectric utilization. The solar energy heat utilization technologies in buildings include solar stoves, solar hot water, solar heating (active and passive), solar refrigeration, solar wind towers, etc. [5]. Solar hot water and solar heating technology are more suitable prospects for the energy supply system of PSSBs in the Qinghai-Tibet Plateau. Solar heating technology can generally be divided into passive and active solar heating according to the difference in heat collection methods [6]. Passive solar heating mainly uses the main components of the building for solar heat collection and heating. Active solar heating technology is developed based on solar hot water, integrated into the heating system using different functional equipment [7]. Compared with passive solar heating technology, active solar heating technology has the advantages of flexible regulation, high fraction, and reliability [8].

conditions [13]. Huang et al. studied the economic path of a single household SHS with levelized heat cost as an economic evaluation index [14]. A comprehensive economic and environmental evaluation of active SHSs in energy-saving buildings in Greece was performed, and the results show that the SHS bears 45% of the building heat load; the payback period of the system is as low as 4.5 years, and more than 50 t of CO_2 emissions are reduced every year [15]. Hobbi and Siddiqui used TRNSYS simulation software to optimize and analyze the system design parameters of the SHS of a single-family residence in Montreal, Canada, such as the collector area and layout mode, heat medium flow, heat storage volume, and connecting pipeline [16]. Myeong proposed an optimization method of SHS based on life cycle cost (LCC) and used a genetic algorithm to optimize the system design parameters [17]. The results show that the system design parameters under the minimum LCC can be determined by trade-offing between equipment and energy costs. According to the actual operation of commercial buildings, Qiu et al. proposed a solar time-sharing heating control strategy, which can effectively reduce the investment payback period of a SHS [18]. Villasmil et al. studied the effects of different flow control strategies on seasonal heat storage coupled with solar SHS performance, and results show that the low flow control strategy can reduce the required storage volume by 35% [19]. Wang et al. proposed a novel feedback control strategy for a combined heating system consisting of a solar collector and air source heat pump (ASHP). Compared with the “constant temperature” strategy, the novel strategy can improve the system’s working efficiency and solar guarantee rate [20].

1.2. Building integrated photovoltaic

Photovoltaic (PV) systems convert solar radiation into higher-grade electric energy. The electricity generated can meet almost all the building energy consumption requirement grades. Hence, integrating a PV system with building facades and the energy consumption system has broad application prospects. Long-term and continuous research has been carried out on Building Integrated PV (BIPV) technology. The integration pattern of building and photovoltaic mainly includes PV walls, PV roof, PV curtain walls, PV external windows, PV sun shading, etc. [21]. Singh et al. analyzed the

thermoelectric performance when using PV modules as building materials for walls and roofs. They found that PV walls and roofs have better thermoelectric benefits when combined with electric air conditioning devices with a high-performance coefficient [22]. Peng et al. proposed a new type of C-Si-based PV window. The experimental results show that the new PV window efficiently generates power, reduces the solar thermal gain coefficient, and effectively reduces uncomfortable glare [23]. Sun and Yang comprehensively analyzed the power generation and load reduction performance of building window photovoltaic shading devices, and the best inclination angle of an external window photovoltaic shading in Hong Kong was suggested [24].

1.3. Solar photothermal photovoltaic integration

Solar photothermal (PT) and photovoltaic (PV) integrated technologies have attracted increased research recently to meet a building's comprehensive heat and electric energy needs. The integration forms mainly include PV and passive building modules, PV and PT devices, PV electric systems, and solar heat collection systems. Ji et al. proposed a novel PV-Trombe wall to directly heat the room and use the generated power for lighting and other electrical appliances [25]. The experimental results show that room temperature is maintained at about 13.4 °C near the PV-Trombe wall throughout the day, and the electrical efficiency of PV can be improved by 5.0%. Arslan et al. designed a new type of finned air-fluid photovoltaic-thermal collector [26]. Experimental research determined that the photovoltaic air collector's comprehensive thermoelectric energy and exergy efficiency can reach 40.6% and 63.5%, respectively. Barbu et al. performed numerical simulation and analysis on the thermoelectric coupling performance of liquid-based photovoltaic thermal (PVT) module, and the results show a general thermoelectric performance compromise in PVT devices [27]. Wang et al. analyzed the operation performance of PV and solar hot water heating coupling systems, but the PV system only provides power to the circulating water pump [28]. The results show that the PV and solar hot water heating coupling system can work normally without a controller, and the solar irradiance started by the circulating water pump has an essential impact on the system's thermal efficiency.

Moreover, many studies have focused on applying integrated PVT devices in building energy systems for the research on PV and PT integrated energy supply systems in buildings. Behzadi et al. designed a system composed of PVT and heat storage tank applied to intelligent buildings. The optimization results show that the cost of building electric and thermal energy using PVT systems is reduced by 16.7 €/MWh and 7.7 €/MWh, respectively [29]. Herrando et al. compared a PVT-based CCHP system with the single PT and PV systems. The results show that the PVT-CCHP system can undertake more building load and reduce carbon emissions [30]. Kavian et al. analyzed the comprehensive performance of PVT and ground source heat pump hybrid systems in terms of energy, economy, and environment. They determined that the traditional ground source heat pump system has a lower investment payback period and significant energy conservation and environmental protection [31].

1.4. Solar thermal and electricity storage

The energy storage devices play a role in adjusting the balance of supply and demand in the solar energy supply system (SESS), which positively affects the solar energy guarantee rate. To ensure a continuous energy supply of the solar energy collection system, Alptekin and Ezan studied the performance of the solar heat collection system equipped with a sensible heat energy storage tank. They showed that increasing the tank height can improve the stratification effect of the water tank and improve the efficiency of the heat collection system [32]. Zhao et al. analyzed the energy-saving performance of an SHS with a phase change energy storage box. They determined that, compared with SHSs, the energy-saving capacity of SHS with PCM heat storage box increases by 34% [33]. Ucar and Inalli conducted a comparative study on the thermal performance and economic benefits of three seasonal heat storage solar central heating systems. The results show that the underground

heat storage system can increase solar energy utilization and the energy-saving effect [34].

A battery is the most used energy storage method for solar photovoltaic systems. Sharma et al. studied the building integrated photovoltaic system with batteries and showed that the building integrated photovoltaic system with batteries has a better economic value under the constraints of a power grid [35]. For zero energy consumption photovoltaic buildings, Vieira et al. studied the effect of lithium-ion batteries in a photovoltaic energy supply system. The results show that the batteries increase the matching degree between photovoltaic power generation and building energy consumption [36].

To summarize, the current research on solar heating and power generation in buildings mainly includes equipment performance improvement, energy conservation and economic analysis, system optimization design, and operation control strategy. These studies provide a foundation for designing and applying solar energy systems in public sanitation service buildings. However, the following aspects are insufficient and need further research:

- The current research on integrating solar photothermal and photovoltaic mainly focuses on a solar system with photovoltaic collectors as the core component. Although the PVT module can output heat and electricity simultaneously, the fixed output proportion of heat and electricity leads to a gap in applications to buildings with different energy consumption characteristics. A hybrid system composed of independent photovoltaic cells and collectors has the advantage of flexible matching of the heat and power demand. However, there is a lack of research on the optimal design and performance comparative analysis of a hybrid system.
- The existing research has studied capacity optimization and control of single solar heating, photovoltaic power generation, and photovoltaic integrated photothermal system. However, few studies have comprehensively discussed and compared the performance and applicability of independent solar systems and different integrated photothermal photovoltaic systems.
- There are significant differences in energy load composition, energy consumption intensity, and duration between public sanitation service buildings and traditional public buildings. At present, there is a lack of analysis on the energy consumption characteristics of public sanitation service buildings and the optimal design and performance evaluation of solar energy supply systems applied to public sanitation service buildings.

The following research work has been carried out to address the shortcomings of existing research in this study. Firstly, eight potential forms of SESSs are proposed, and the corresponding operation strategies are put forward based on the analysis of the energy consumption characteristics of PSSBs. Then, an optimization simulation model of the SESSs with LCC minimum as the objective function is developed, and the corresponding model solution method is given. Thirdly, taking the PSSB in Lhasa, Tibet, as a case study, the dynamic operation performance, annual energy conservation, economy, and CO₂ emission reduction performance of different systems are analyzed. Finally, the sensitivity of economic parameters and equipment price to system optimization results are discussed and compared. The results provide a reference for the optimization and design of solar energy supply systems for PSSBs.

2. Solar energy systems for public sanitation service buildings

There are a variety of potential solar energy systems that could be implemented in PSSBs. In this part, firstly, the energy demand and supply mode of the PSSBs are introduced. Secondly, according to the energy consumption characteristics of the PSSBs, eight different solar energy systems are proposed, and the principles of each system are introduced. Finally, the

2.1. Energy demand and solar energy supply mode

The energy demand of the PSSBs and energy supply mode are shown in Fig. 2. According to the main functions of the PSSBs, their energy consumption mainly includes heat and power. Heat consumption is generated by space

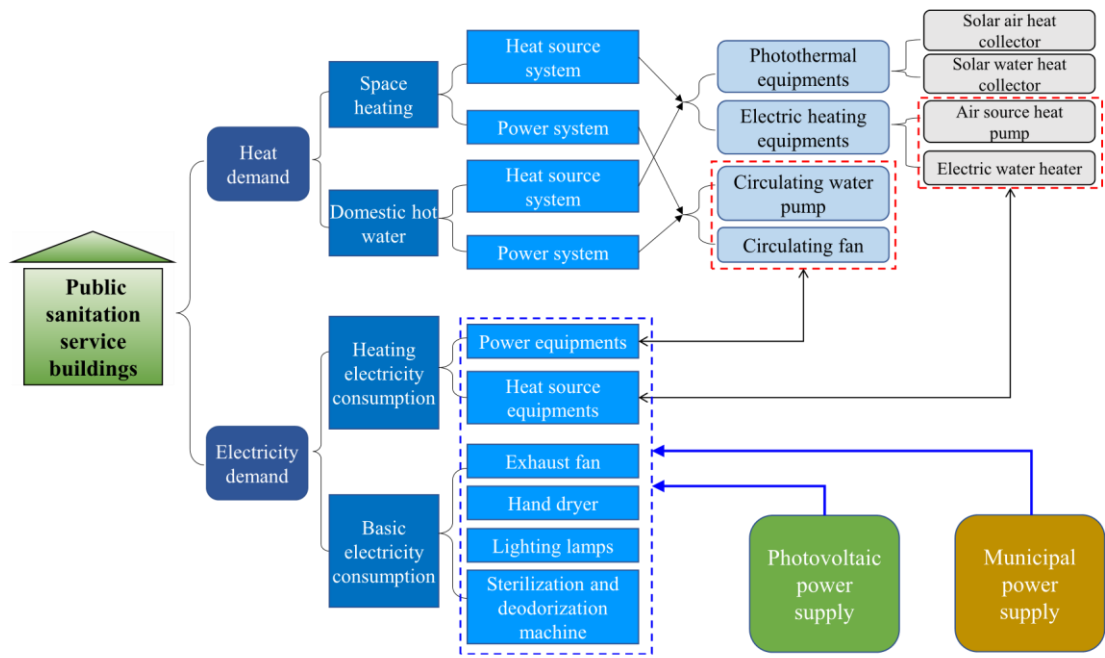


Fig. 2. Energy demand and energy supply mode of PSSBs.

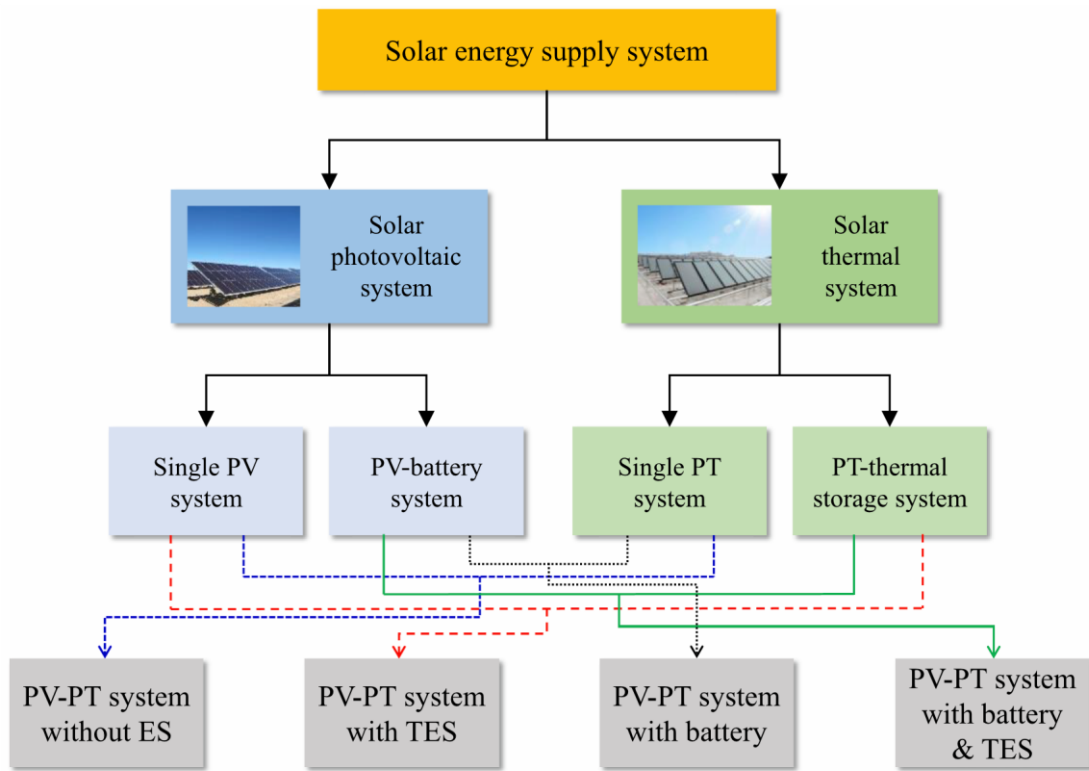


Fig. 3. Solar energy supply system for PSSBs.

operation control strategy of each system is introduced.

heating and domestic hot water. The electric power consumption consists of essential power consumption (exhaust fan, hand dryer, lighting lamps, and sterilization/deodorization machine) and heat power consumption (heat source equipment, circulating pump, and fan). For the PSSBs in solar energy-

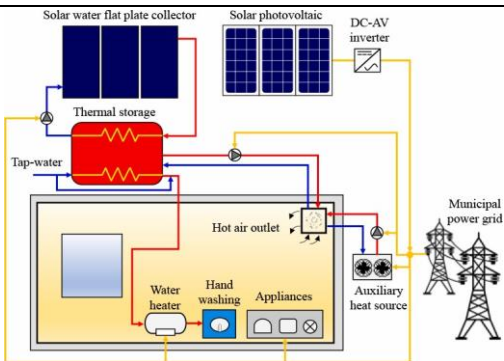
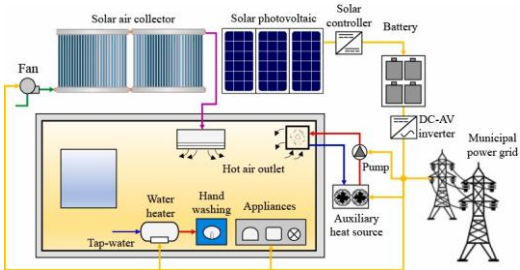
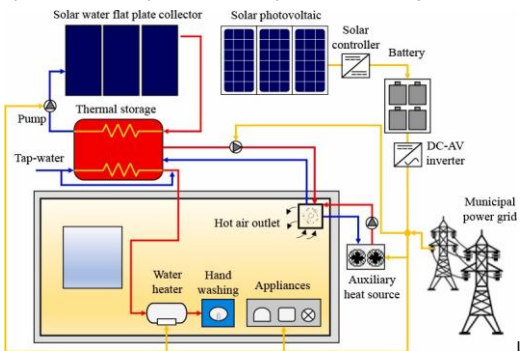
rich areas, solar heat collection systems can meet space heating and domestic hot water energy

Table 1
Principles and characteristics of different types of SESSs.

System schematic diagram	System characteristics
<p>System I: Single PV system</p>	<p>a. The electric power is provided by the PV system and power grid. b. Due to without power storage device, all the electrical load is undertaken by the power grid when the photovoltaic power supply is insufficient. c. The air source heat pump and electric water heater are used as the heat source of the heating subsystem, and the hot water subsystem, respectively.</p>
<p>System II: Single PT system</p>	<p>a. The heating energy is supplied by the solar hot air collection system. b. The electric and hot water load is undertaken by the power grid. c. Due to without thermal storage device, the municipal power will drive the auxiliary heat source for heating when the heat supply of the solar air heat collection system is insufficient.</p>
<p>System III: PV + battery system</p>	<p>a. The PV system and power grid jointly supply power to energy consuming devices. b. The power will be stored in the battery when the power generation of PV is excessive, and the battery will priority supply power to system when the power supply of PV is insufficient. c. The air source heat pump is used for space heating, and the electric water heater is used supply domestic hot water.</p>
<p>System IV: PT + thermal storage system</p>	<p>a. The energy for heating and hot water is supplied by the solar hot water collector system. b. The heat will be stored in the water tank when the solar heat collection is excessive, and the water tank will priority supply heat to the system when the heat supply of the system is insufficient. c. The power load is undertaken by the power grid, and the municipal power will drive the auxiliary heat source for heating when the heat supply of the solar heat collection system is insufficient.</p>
<p>System V: PV-PT system without energy storage</p>	<p>a. The heating energy is supplied by the solar hot air collection system. b. The energy for electrical equipment and hot water is supplied by the PV system and power grid. c. Due to without energy storage device, the whole heat and electrical loads are undertaken by power grid when the energy supply of the solar system is insufficient.</p>
<p>System VI: PV-PT system with thermal storage</p>	

(continued on next page)

Table 1 (continued)

System schematic diagram	System characteristics
	<p>a. The energy for heating and hot water is supplied by the solar hot water collector system.</p> <p>b. The power load and partial heat load are undertaken by the PV system and power grid.</p> <p>c. The heat will be stored in the water tank when the solar heat collection is excessive, and the water tank will priority supply heat to the system when the heat supply is insufficient.</p> <p>d. The municipal power will drive the auxiliary heat source to ensure the reliable operation of the system.</p>
<p>System VII: PV-PT system with battery</p> 	<p>a. The heating energy is supplied by the solar hot air collection system.</p> <p>b. The energy for electrical equipment and hot water is supplied by the PV system and power grid.</p> <p>c. The power will be stored in the battery when the power generation of PV is excessive, and the battery will priority supply power to system when the power supply of PV is insufficient.</p> <p>a. The energy for heating and hot water is supplied by the solar hot water collector system.</p> <p>b. The power load and partial heat load are undertaken by the PV system and power grid.</p> <p>c. The heat and power will be stored in the water tank and battery when the energy collection of solar system is excessive, and the energy storage devices will priority supply energy to the system when the energy is insufficient.</p> <p>d. The municipal power will drive the auxiliary heat source to ensure the reliable operation of the system.</p>
<p>System VIII: PV-PT system with battery and thermal storage</p> 	<p>Legend of air, water, and electric power lines</p> <p>→ Outdoor air → Hot air → Low temperature water → Electricity → High temperature water</p>

consumption. The PV system can meet the basic power consumption and the heating power demand of power and heat source equipment. Due to the instability of solar energy, the electric power needs to be supplemented by the municipal power grid to ensure the system's stable operation. The utilization proportion of renewable energy should be increased to reduce the impact of the energy system on the environment. Therefore, the solar fraction of the system should be improved to reduce the conventional power consumption when designing the SESS of PSSBs. 2.2. Solar energy supply system scheme

The SESS is divided into solar PV and PT systems according to the energy output type, as shown in Fig. 3. If there are energy storage devices, the solar PV system is divided into a single PV system and a PV with electrical energy storage (EES) system. The PT system is divided into a single PT system and PT with thermal energy storage (TES) system. The PT and PV systems are then combined to form a PV-PT system, a PV-PT with TES system, a PV-PT with EES system, or a PV-PT with EES and TES system. Overall, according to the solar PV

and PT combination and if an energy storage device is present, eight potential forms of SESS for PSSBs can be implemented.

The schematic diagrams and descriptions of the above eight SESSs and the corresponding system features are shown in Table 1.

2.3. Operation strategy

Current studies indicate that unstable PV power generation has a different impact on the power quality of the grid and equipment when a small-scale distributed PV power generation system is connected to the public power grid [37]. Considering the small scale and high dispersion of PV power generation in PSSBs in Tibet, this study assumed that the system takes electricity from the municipal power grid, and the remaining PV power generation is not transmitted to the grid. The following principles are also followed: (1) PV power generation prioritizes use and consumption compared to municipal power to improve the penetration of renewable energy. (2) Compared with PV/municipal power heating, the heat collection and storage of the PT system has a higher priority to improve the energy conversion efficiency of the system.

When the PT system's solar heat collection and storage cannot meet the heat demand, PV power generation and electric heating conversion supplements are given priority, and municipal power is finally considered. (3) If the instantaneous PV power generation is greater than the power demand and the system is equipped with a battery, it is preferred to store electricity through the battery. Excess power is released if the battery is full or there is no battery. According to the above principles, the operation strategies of different forms of SESSs for PSSBs in the Tibet Plateau are put forward, as shown in **Supplementary A**.

proposed, as shown in Fig. 4. Firstly, the building energy simulation software Energy Plus simulated the buildings' heating load, hot water load, and power load to provide essential input parameters for system optimization. Secondly, according to the energy balance process of each system and the mathematical model of each equipment component, the thermal process mathematical model of the SESS was established and solved by the TRNSYS simulation platform. Then, the system equipment capacity optimization models aimed at LCC were established, including corresponding decision variables and constraints, and the optimization simulation calculation is carried out in

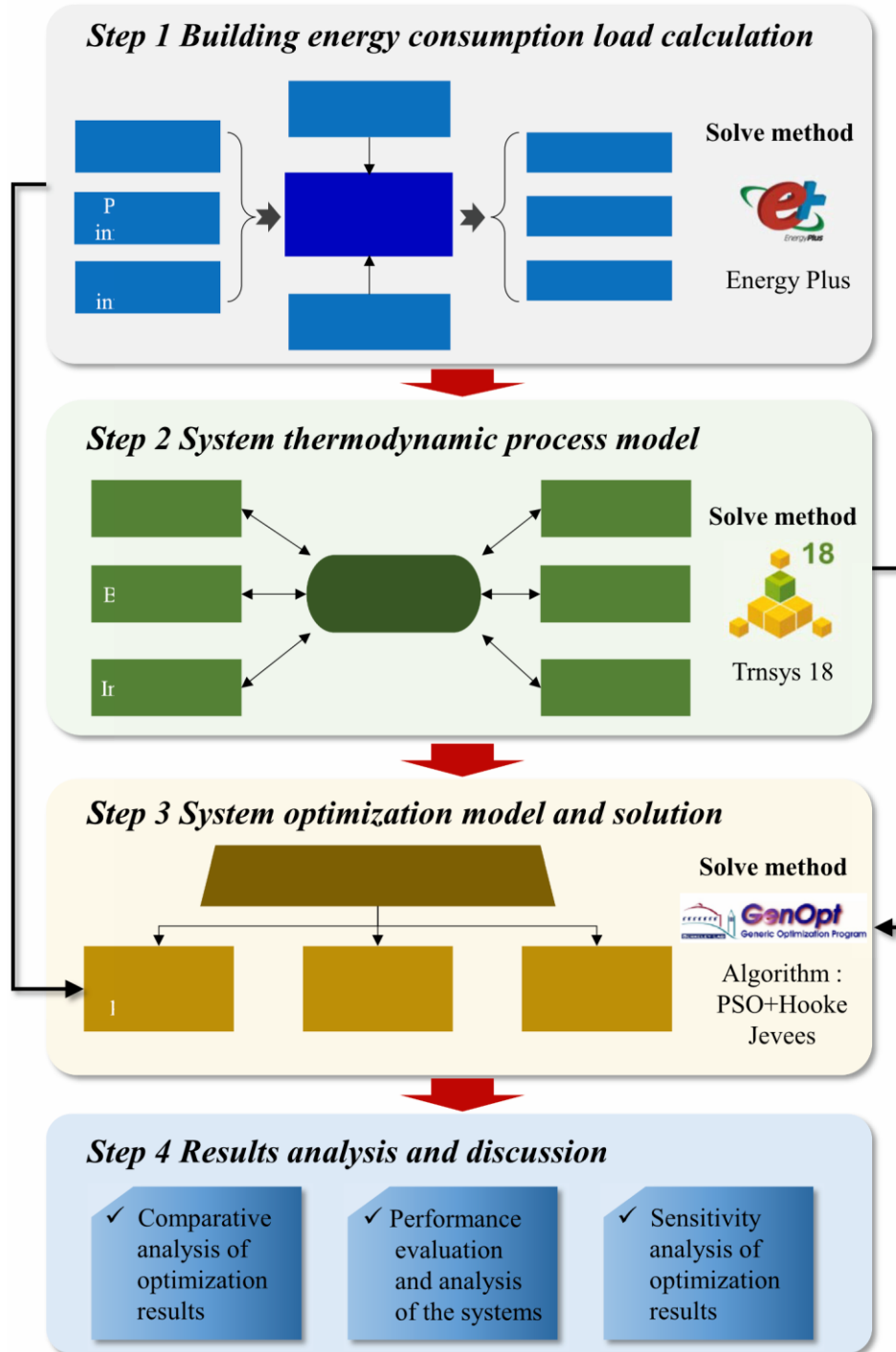


Fig. 4. Research Method and Routine.

3. Methods

To compare and analyze the operating performance of the eight potential SESSs for PSSBs in the Tibet Plateau, the method framework of this study is

combination with TRNSYS and GenOpt platform. Finally, the simulation and optimization results of different systems were analyzed and discussed, including comparing and analyzing the energy conservation and economy of different system schemes, analyzing the sensitivity of optimization results to

setting parameters and discussing the operation characteristics and life cycle benefit evaluation of different systems. The details are described below.

Table 2

Transient energy balance equation of SESS.

Type	Energy balance equation
System I	Electricity $\int e_{PV}(t) + \int e_{Grid}(t) = \int e_{BE}(t) + \int e_{PE}(t) + \int e_{ASHP}(t) +$
System II	Heat $\int q_{ASHP}(t) + \int q_{EH}(t) = \int q_{Heat}(t) + \int q_{Water}(t) + \int q_{Loss}(t)$
System III	Electricity $\int e_{EH}(t) + \int e_{Loss}(t) = \int q_{ASHP}(t) + \int q_{EH}(t) = \int q_{Heat}(t) + \int q_{Water}(t) + \int q_{Loss}(t)$
System IV	Heat $\int q_{ASHP}(t) + \int q_{EH}(t) = \int q_{Heat}(t) + \int q_{Water}(t) + \int q_{Loss}(t)$
System V	Electricity $\int e_{PE}(t) + \int e_{ASHP}(t) + \int e_{EH}(t) + \int e_{Loss}(t) = \int q_{ASHP}(t) + \int q_{EH}(t) = \int q_{Heat}(t) + \int q_{Water}(t) + \int q_{Loss}(t)$
System VI	Heat $\int q_{Water}(t) + \int q_{Loss}(t) + \int q_{TES}(t) = \int e_{PV}(t) + \int e_{Grid}(t) = \int e_{BE}(t) + \int e_{PE}(t) + \int e_{ASHP}(t) + \int e_{EH}(t) + \int e_{Loss}(t)$
System VII	Electricity $\int q_{ASHP}(t) + \int q_{EH}(t) = \int q_{Heat}(t) + \int q_{Water}(t) + \int q_{Loss}(t)$
System VIII	Heat $\int q_{Water}(t) + \int q_{Loss}(t) + \int q_{TES}(t) = \int e_{PV}(t) - \int e_{Cha}(t) + \int e_{Dis}(t) + \int e_{Grid}(t) = \int e_{BE}(t) + \int e_{PE}(t) + \int e_{ASHP}(t) + \int e_{EH}(t) + \int e_{Loss}(t)$

Note: e_{PV} is the electricity generation of the photovoltaic system; e_{Grid} is the electricity provided by the municipal power grid; e_{BE} is the electricity consumption of basic equipment; e_{PE} is the electricity consumption of power equipment; e_{ASHP} is the electricity consumption of the air source heat pump; e_{EH} is the electricity consumption of the electrical heater; e_{Cha} is the electric charge of the battery; e_{Dis} is the electricity discharge of the battery; e_{Loss} is the electricity loss; q_{Heat} is the thermal consumption of space heating; q_{Water} is the thermal consumption of hot water; q_{SC} is the heat supply of the solar collector; q_{EH} is the heat supply of the electric heater; q_{ASHP} is the heat supply of the air source heat pump; q_{TES} is the heat stored/released in the water tank; q_{Loss} is the heat loss of the system.

3.1. Mathematical model

An accurate system mathematical model is the basis of system operation characteristic analysis and optimization design. The thermal process mathematical model of the solar energy supply system in PSSB is composed of the energy balance equation of each system and the equipment models of solar collector, heat storage tank, PV module, battery, and ASHP.

3.1.1. Energy balance equation

For the above-mentioned eight solar energy systems, the law of energy balance between the input and output of each part of the system is the basic rule for reasonable operation of each system. Based on the energy transfer process analysis during the system operation, each system's dynamic energy balance equation was developed, as shown in Table 2. Each system's transient energy balance equation consists of the electricity and heat balance equations.

3.1.2. Solar collector

A solar collector is the core device in an SHS, and its performance directly affects the heat supply and system efficiency. Heat collection by solar collectors is expressed as a function of the tilted surface radiation, effective heat collection area, and collector efficiency. The solar heat collection can be calculated as follows:

$q_{SC}(t) = G_T(t) A_{SC} \eta_{SC}(t)$ (1) where G_T is the total tilted surface radiation of the solar collector, $W \cdot m^{-2}$; A_{SC} is the effective heat collection area of the solar collectors, m^2 ; η_{SC} is the solar collector efficiency.

The performance of the solar collector is usually measured by its heat collection efficiency. Collector efficiency is based upon material characteristics and is mainly affected by solar radiation intensity and ambient temperature. The calculation formula of the solar collector efficiency is as follows: [38]:

$$\eta_{SC}(t) = \eta_0 - a_1 T^*(t) - a_2 G_T(t) (T^*(t))^2 \quad (2)$$

$$T^*(t) = T_{in}(t) - T_{amb}(t) \quad (3)$$

$G_T(t)$ where, T^* is the normalized temperature difference, $m^2 \cdot ^\circ C \cdot W^{-1}$; T_{in} is the inlet temperature of the collector, $^\circ C$; T_{amb} is ambient temperature, $^\circ C$; η_0 is the collector thermal efficiency at $T^*=0$; a_1 is the first-order efficiency coefficient of heat collection efficiency; a_2 is the second-order efficiency coefficient of heat collection efficiency.

3.1.3. Heat storage tank

A heat storage tank is a standard energy storage device in an SHS. Due to water density variations at different temperatures, the water temperature in a hot water storage tank is stratified during the system operation. This study adopted the layered heat storage tank model, assuming that the water in the tank is divided into i layers, and the energy balance equation of node i is as follows [39]:

$$\frac{dT_i}{dt} = \frac{UA_T}{m_i c_p} (T_{amb} - T_i) + \frac{1}{m_i c_p} \left(\int_{T_{i-1}}^{T_i} m_{i-1} (T_{i-1} - T_i) dT + m_{i-1} (T_{i-1} - T_i) + m_{i+1} (T_{i+1} - T_i) \right) \quad (4)$$

where, U is the surface heat transfer coefficient of the water tank, $W \cdot m^{-2} \cdot K^{-1}$; A_T is the surface area of the water tank in contact with the environment, m^2 ; c_p is the constant pressure specific heat capacity of water, $kJ \cdot kg^{-1} \cdot K^{-1}$; m_{ST} is the

flow rate of the solar heat collection system, $\text{kg}\cdot\text{h}^{-1}$; T_{ST} is the outlet temperature of the solar collector, $^{\circ}\text{C}$; m_{HL} is the flow rate of the heating system, $\text{kg}\cdot\text{h}^{-1}$; T_{HL} is the return temperature of the heating system, $^{\circ}\text{C}$; m_{WL} is the flow rate of the hot water system; T_{WL} is the mains water temperature, $^{\circ}\text{C}$; T_i is the average water temperature of node i of the heat storage tank, $^{\circ}\text{C}$.

3.1.4. Photovoltaic cell

A PV cell converts absorbed solar energy into electric energy through the PV effect. The energy conversion efficiency is related to its characteristics, ambient temperature, and solar radiation intensity. In this study, the PV cell adopted a polycrystalline silicon PV cell. The formula for PV cell power generation is as follows [40]:

$$e_{\text{PV}}(\tau) = Y_{\text{PV}} f_{\text{PV}} [1 + \alpha_p (T_c(\tau) - T_{\text{c,STC}})] G_{\text{T,STC}} \quad (5)$$

where, Y_{PV} is the rated power of PV cells, kW; f_{PV} is the PV derating factor (it is assumed as 85%, including 5% panel surface loss and 10% energy loss); T_c is the

Frosting area	Defrosting cycle /min	Frosting-defrosting loss efficiency κ
$\geq 0.1189T_a^2 - 1.84T_a + 82.64$	20	36%
$\geq 0.0698T_a^2 - 1.09T_a + 69.28$	30	35%
$RH \geq 0.065T_a^2 - 0.85T_a + 58.29$	40	31%
$RH \geq 0.0157T_a^2 - 0.66T_a + 44.27$	50	24%
$< 0.0157T_a^2 - 0.66T_a + 44.27$	/	0

where, $NOCT$ is the normal operating cell temperature, $^{\circ}\text{C}$. In this study, $NOCT$ is taken as 42°C .

3.1.5. Battery

The battery is the energy storage device in the PV power generation system, which converts the direct current from PV into chemical energy and stores it. When the PV power generation is in surplus, the battery is charging, and when the PV power generation is insufficient, the battery is discharging. The instantaneous power E_{Bat} is related to the battery state of charge or discharge and can be calculated as [42]:

$$\text{Charging: } E_{\text{Bat}}(\tau) = E_{\text{Bat}}(\tau - \Delta\tau) (1 - S_d) + P_c \eta_b \Delta\tau \quad (7)$$

$$\text{Discharging: } E_{\text{Bat}}(\tau) = E_{\text{Bat}}(\tau - \Delta\tau) (1 - S_d) - P_d(\tau) / \eta_d \Delta\tau \quad (8)$$

where, E_{Bat} is the remaining electric energy in the battery, kWh; S_d is the self-discharge factor [43]; P_c and P_d are the battery charging and discharging power, kW. η_c and η_d are the charging and discharging efficiencies. In this study, charging efficiency is equal to discharging efficiency [44].

The state of charge (SOC) of the battery during the charging and discharging processes can be calculated as:

$$E^{\text{Bat}}(\tau)$$

$$\text{SOC}(\tau) = \frac{E^{\text{Bat}}(\tau)}{C_{\text{Bat}}} \quad (9) \quad \text{where, } C_{\text{Bat}} \text{ is the battery capacity, kWh. The}$$

battery stops charging when SOC reaches the upper limit of 1 and stops discharging when the SOC reaches the lower limit of 0.3.

3.1.6. Air source heat pump

An air source heat pump (ASHP) is efficient heating equipment that converts low-grade heat energy in the air into high-grade heat energy that can be used for heating through the electric drive. The heating efficiency of

PV module instantaneous temperature, $^{\circ}\text{C}$; $T_{\text{c,STC}}$ is the PV cell temperature under STC, $^{\circ}\text{C}$; α_p is the PV temperature coefficient for the power (α_p of a polycrystalline silicon PV cell is $-0.48\% \cdot ^{\circ}\text{C}^{-1}$ [41]).

The PV module's instantaneous temperature can be attained by:

$$G^{\text{T}}(\tau)(NOCT - 20)$$

$$T_c(\tau) = T_{\text{amb}}(\tau) + \frac{G^{\text{T}}(\tau)(NOCT - 20)}{800} \quad (6)$$

Table 3

Frosting-defrosting loss efficiency of ASHP under different frosting conditions [45].

Table 4

Decision variables corresponding to different system types.

System type	Variables
System I: Single PV system	APV, P_{ASHP}
System II: Single PT system	ASC, P_{ASHP}
System III: PV + battery system	$APV, P_{\text{ASHP}}, C_{\text{Bat}}$
System IV: PT + thermal storage system	$ASC, P_{\text{ASHP}}, V_{\text{Tank}}$
System V: PV-PT system without energy storage	$APV, ASC, P_{\text{ASHP}}$
System VI: PV-PT system with thermal storage	$APV, ASC, P_{\text{ASHP}}, V_{\text{Tank}}$
System VII: PV-PT system with battery	$APV, ASC, P_{\text{ASHP}}, C_{\text{Bat}}$
System VIII: PV-PT system with battery and thermal storage	$APV, ASC, P_{\text{ASHP}}, C_{\text{Bat}}, V_{\text{Tank}}$

ASHP is mainly related to the outdoor air temperature, relative humidity, and operating temperature. The heating capacity of ASHP can be attained as follows:

$Q_{\text{ASHP}}(\tau) = S_{\text{ASHP}} \cdot E_{\text{ASHP}} \cdot \text{COP}(\tau) \cdot (1 - k)$ (10) where, E_{ASHP} is the power of ASHP, kW; S_{ASHP} is the on and off control signal of the ASHP, and 1 represents the point when the ASHP starts running, and 0 indicates that the ASHP stops running.

The coefficient of performance (COP) of ASHP under heating mode can be calculated as [45]:

$$\text{COP}(\tau) = 1.189 \times 10^{-4} T_{\text{amb}}(\tau)^2 + 0.0546 T_{\text{amb}}(\tau) + 3.41 \quad (11)$$

The evaporator coil of the ASHP frosts when the relative humidity corresponding to the outdoor temperature is greater than a specified value, which affects the operation performance of the ASHP. Therefore, the loss coefficient of frosting and defrosting is proposed, which is the ratio of the frosting performance coefficient and the stable coefficient of the ASHP when the outdoor heat exchanger is a dry coil. The defrosting cycle and loss coefficient of the ASHP under different operating modes are shown in Table 3. 3.2. Optimization model and solution

It is important to establish the optimization design model for each system to compare and analyze the differences in operation effects of different system schemes under the same environmental boundary conditions. The optimization model consists of decision variables, objective functions, and constraints.

3.2.1. Decision variables

The capacity parameters of the equipment in the system were used as decision variables. The decision variables mainly include PV area APV , solar collector area ASC , ASHP power P_{ASHP} , the rated power of the battery N_{Bat} , and heat storage tank volume V_{Tank} . Due to each system's different constituent equipment, the decision variables of each system are different, as shown in Table 4.

3.2.2. Objective function

The economic cost is an essential factor affecting the system design scheme, so LCC was used as the objective function to optimize the equipment capacity of several proposed systems. LCC includes the initial investment, replacement cost, operation, and maintenance cost within the system operation process, and system salvage value after the expiration of the system, which can be calculated as follows [46,47]:

$LCC = C_{IN} + C_{OM} + C_{RE} - C_{SV}$ (12) where, C_{IN} is the initial investment of the system, CNY; C_{RE} is the replacement cost, CNY; C_{OM} is the operation and maintenance cost within the system operation process, CNY; C_{SV} is the system salvage value, CNY.

$$C_{OM} = \sum_{t=0}^N \frac{1+f}{d} [EP \cdot AEC] + (C_{IN} + C_{RE}) \times \mu \quad (13)$$

$$C_{RE} = C_{Bat} \cdot \left[\left(\frac{1+f}{1+d} \right)^5 + \left(\frac{1+f}{1+d} \right)^{10} + \left(\frac{1+f}{1+d} \right)^{15} \right] \quad (14)$$

$$C_{SV} = (C_{IN} + C_{RE}) \times \varphi \quad (15)$$

where, AEC is the annual energy consumption of the system, kWh; EP is the municipal electricity price, CNY·kWh⁻¹; μ is the ratio of equipment maintenance cost to equipment purchase cost (2%); f is the annual inflation rate, %; d is annual interest rate, %; φ is system salvage value ratio. N is the system design life cycle, year.

The value of the system salvage value ratio is usually between 3% and 5%; 4% was used in this study [48]. The life cycle was taken as 20 years, and the battery's life was 5 years, so the replacement cost needed to be calculated [49].

3.2.3. Constraint condition

Constraints are critical to ensure reasonable and practical calculation

Table 5
Main technical parameters of components in the TRNSYS model.

Number	Equipment	Component	Main setting parameters
1	Solar hot water collector	Type 71	$\eta_{SC} = 0.514 - 2.154 \times T^* - 0.0126 \times (T^*)^2$; Fluid specific heat: 4.174 kJ·kg ⁻¹ ·K ⁻¹ .
2	Solar hot air collector	Type 71	$\eta_{SC} = 0.654 - 2.385 \times T^*$; Fluid specific heat: 1.005 kJ·kg ⁻¹ ·K ⁻¹ .
3	Photovoltaic panel	Calculator	Rated power of PV cells per unit area, 168.75 Wm ⁻² ; α_p of polycrystalline silicon PV cell is -0.48%·°C ⁻¹ .
4	Heat storage tank	Type 156	Tank height, 3.5 m; Number of tank nodes, 3; Loss coefficient, 0.7 Wm ⁻² ·K ⁻¹ .
5	Inverter	Type 48	Regulator efficiency, 0.94; Inverter efficiency, 0.92; High limit on FSOC, 1; Low limit on FSOC, 0.3; Charge to discharge limit on FSOC, 0.1.
4	Battery	Type 47a	Charging efficiency, 0.9.
5	Electric heater	Type 138	Efficiency, 0.9; Rate power, 9.2 kW.
6	Air source heat pump	Type 700 Calculator	Set point temperature, 45 °C; $COP = 1.189 \times 10^{-4} T_{amb}^2 + 0.0546 T_{amb} + 3.41$.
9	Circulating pump	Type 114	Rated flow rate; Rated power; Fluid specific heat: 4.174 kJ·kg ⁻¹ ·K ⁻¹ .
10	Fan	Type 146	Rated flow rate; Rated power; Fluid specific heat: 1.005 kJ·kg ⁻¹ ·K ⁻¹ .

results of the optimization model. The optimization model constraints consist of the energy balance equality constraints and parameter value inequality constraints. The energy balance equation constraints of all systems are shown in Table 2. In addition, the value range of decision variables of each system is as follows:

$$0 \leq A_{PV} + A_{SC} \leq A_{max} \quad (16)$$

$$Q \leq P_{ASHP} \leq \frac{Q_{load,max}}{COP_{ASHP}} \quad (17)$$

$$0 \leq C_{Bat} \leq C_{Bat,max} \quad (18)$$

$$SOC_{min} \leq SOC \leq SOC_{max} \quad (19)$$

$$0 \leq V_{Tank} \leq V_{Tank,max} \quad (20)$$

where, A_{max} is the maximum installation area of the roof, m²; $Q_{Load,max}$ is the maximum hourly heating load of a building, kW; $C_{Bat,max}$ is the maximum battery capacity, kW; $V_{Tank,max}$ is the maximum heat storage volume of a heat storage tank, m³.

3.2.4. Solution method

Each system's simulation models were established in the TRNSYS platform according to the thermal process mathematical model of the solar energy supply system. The above optimization model was solved by combining TRNSYS and GenOpt software. The HVAC system diagrams developed by TRNSYS of the eight solar systems are shown in Supplementary B. The main technical parameters of the components in the TRNSYS model are shown in Table 5.

Particle swarm optimization (PSO) is a standard intelligent algorithm for system optimization. However, it is easy to fall into local optimization, and the algorithm has slow convergence in the later optimization stage. The Hooke Jeeves algorithm is a pattern search algorithm with the advantages of fast convergence and strong adaptability. The Hooke Jeeves algorithm is especially suitable for a case with few optimization variables. However, the initial values require high accuracy. If the initial value is inaccurate, it is easy to fall into local optimization [50]. In this study, PSO and Hooke Jeeves algorithms were combined to solve the system optimization model; the calculation flow of the hybrid algorithm is shown in Fig. 5. Firstly, the PSO algorithm was used to calculate the optimal range in space, and then the Hooke algorithm was used to search the pattern in the optimal range to obtain the optimal value.

In the PSO optimization stage, the particle swarm was initialized randomly, including random position and velocity. For each particle, its fitness value was compared with the fitness value of the best position experienced, and the better value was the individual historical optimal value of the particle. Finally, the optimal historical value of each particle was compared with the best position experienced in the group or neighborhood, and the better value was selected as the optimal global value [51].

In the Hooke Jeeves optimization stage, detection search and mode movement were the main processes. After cycle processing (detection search), if the final objective function value decreased compared with that before the cycle, the decision variable was taken as the new base point, and the mode moved to obtain the minimum value of the objective function.

The combination of the two optimization algorithms enhanced the convergence ability of the algorithm and avoided the premature convergence of the algorithm. The Genopt software called the PSO + Hooke Jeeves hybrid algorithm for optimization analysis.

3.3. Assessment indicators

To effectively evaluate and analyze the operating performance of different SESSs, the annual energy saving rate, cost-saving rate, and carbon dioxide emission reduction rate were set as the system performance evaluation indicators. The municipal power grid energy supply system was used as the contrast system. The system schemes were compared and analyzed from energy conservation, economic, and environmental perspectives.

(1) Energy conservation evaluation.

The annual energy saving ratio (AESR) is the ratio of the difference between the energy consumption of the basic system and the SESS to the energy consumption of the contrast system. It can be calculated as follows [52]:

$$AESR = \frac{E_{Con} - E_{SS}}{E_{Con}} \quad (21)$$

where, E_{Con} is the annual electricity consumption of the contrast system, kWh; E_{SS} is the annual electricity consumption of the different SESSs, kWh.

(2) Economy evaluation.

The life cycle cost saving rate (LCCSR) is the ratio of the difference between the LCC of the contrast system and the SESS to the LCC of the contrast system. It can be calculated as follows [52]:

$$LCC_{Con} - LCC_{SS}$$

$$LCCSR = \frac{LCC_{Con} - LCC_{SS}}{LCC_{Con}} \quad (22) \text{ where, } LCC_{Con} \text{ is the life cycle cost of the contrast system, CNY; } LCC_{SS} \text{ is the life cycle cost of the SESS, CNY.}$$

(3) Environmental evaluation.

The annual carbon reduction rate (ACRR) refers to the carbon dioxide emission reduction rate of the SESS compared with the contrast system during the annual operation and can be attained as [31]:

$$L_{CO2,Con} - L_{CO2,SS} \quad ACRR = \frac{L_{CO2,Con} - L_{CO2,SS}}{L_{CO2,Con}} \quad (23)$$

where, $L_{CO2,Con}$ is the operating CO₂ emissions volume of the contrast system, m³; $L_{CO2,SS}$ is the operating CO₂ emission volume of the SESS, m³.

The CO₂ emissions caused by the power generation of the municipal power grid can be calculated as follows. A natural gas system is used as the case study here:

$$M_{methane} = 3.6 \times \frac{\rho_{CO2}}{\varphi} \times \frac{AEC}{LHV} \quad (25)$$

where, AEC is the annual energy consumption, kWh; $M_{methane}$ is methane mass consumed in power generation, kg; ρ_{CO2} is the density of carbon dioxide, kg·m⁻³; φ is the energy conversion efficiency (natural gas generator: 40%); LHV is the low heating value of natural gas (47.174 MJ·kg⁻¹); θ_c is the proportion of CO₂ emissions in natural gas (0.2); CM is the mass ratio of CO₂ emitted by methane combustion (2.75 kg·kg⁻¹).

To use the above system model and optimization solution method for optimal design, the evaluation and comparative analysis of a SESS of a typical PSSB in Lhasa, Tibet, was used as a research case to simulate and analyze the application scenarios of different system schemes. The case information includes typical building shape, dimensions and thermal parameters, local meteorological parameters, user statistics, building energy consumption simulation data, and economic cost parameters.

3.4.1. Building information

The building SketchUp model and floor plan of the PSSB in Lhasa are shown

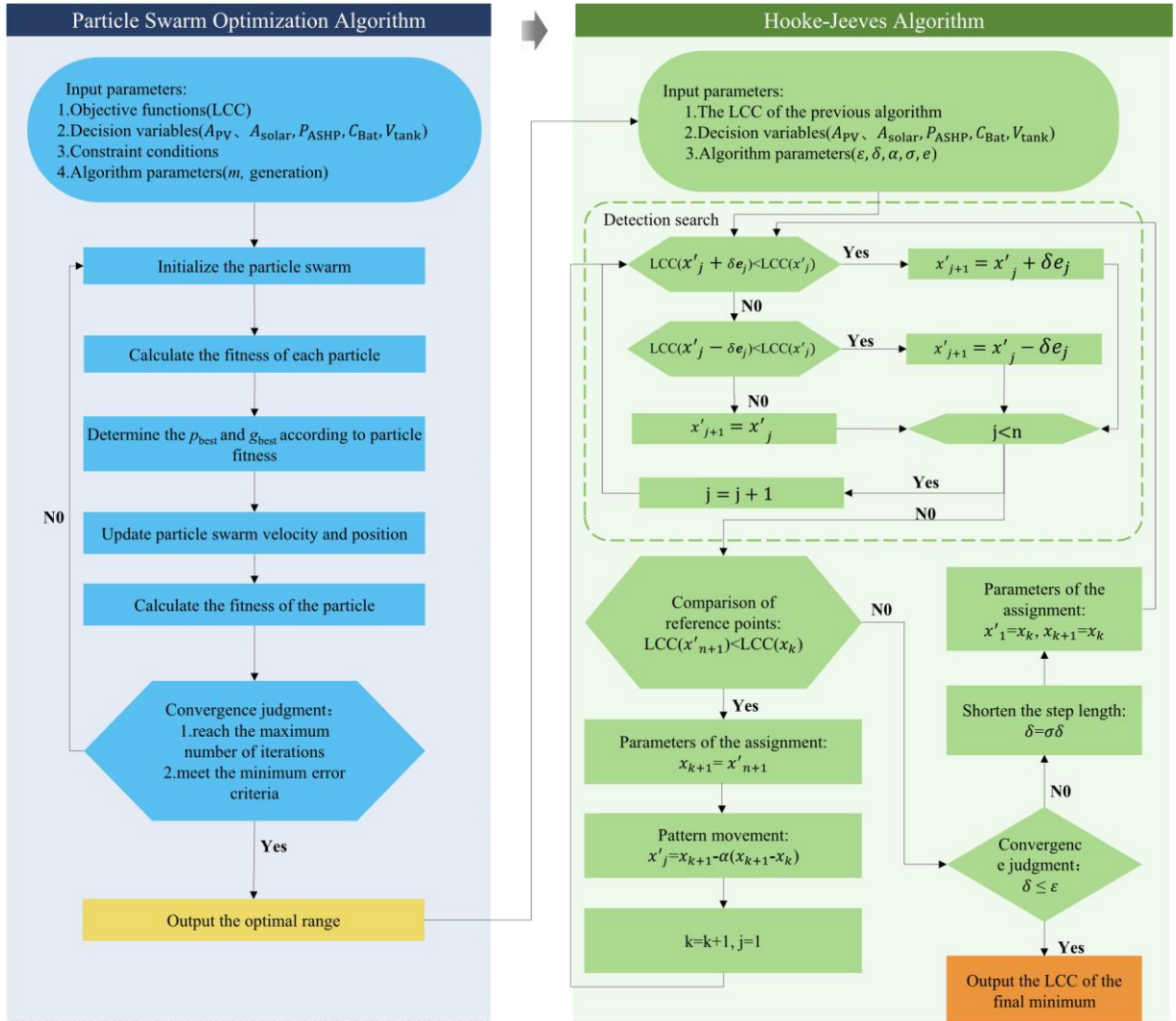


Fig. 5. Optimization model solving logic diagram.

in Fig. 6. The functional area of the building is mainly composed of a female toilet, male toilet, accessible toilet, equipment room, sundry space, and hall.

$$L_{CO2,Grid} = \frac{M_{methane} \times CM}{\rho_{CO2}} \quad (24)$$

The total construction area is 146 m². The envelope parameters and corresponding heat transfer coefficients of the PSSB are shown in Table 6.

3.4.2. Meteorological parameters

The hourly variations of the horizontal solar radiation intensity, outdoor air temperature, wind velocity, and water mains water temperature during typical meteorological years in Lhasa, Tibet, are shown in Fig. 7. The solar radiation and the number of clear-sky days in winter in Lhasa are higher than those during other seasons. In general, solar energy resources are abundant, and the annual total radiation in the horizontal plane is ~7240 MJ·m⁻². The local annual average ambient temperature is 7.54 °C, and the ambient temperature in winter is less than 0 °C for extensive periods, so heating is required during the winter. The ambient temperature is less than 20 °C for most of the summer, so there is no demand for cooling during the summer. The mains water temperature is the crucial parameter for calculating the hot water load. The annual average temperature of tap water is 12.36 °C, with a minimum value of 8.89 °C and a maximum value of 15.82 °C.

Floor	Insulation board	50	2.65
	Heavyweight concrete	200	
Roof	Cement mortar	20	2.71
	Fine aggregate concrete	40	
	Reinforced concrete	200	
Window	Double glass	5 + 9 + 5	3.5

3.4.3. Visitor statistics

The visitor flow of the PSSB is an essential factor affecting the energy consumption of such buildings. This work conducted a short-term test on the passenger flow of a typical public toilet building in Lhasa. The test steps and hourly passenger flow data within a week are shown in Fig. 8. Wireless pedestrian flow sensors were installed at the door of the public toilet, and the sensors relay the signal through Bluetooth. The transmitter records the pedestrian flow data and transmits the data to a terminal program through the

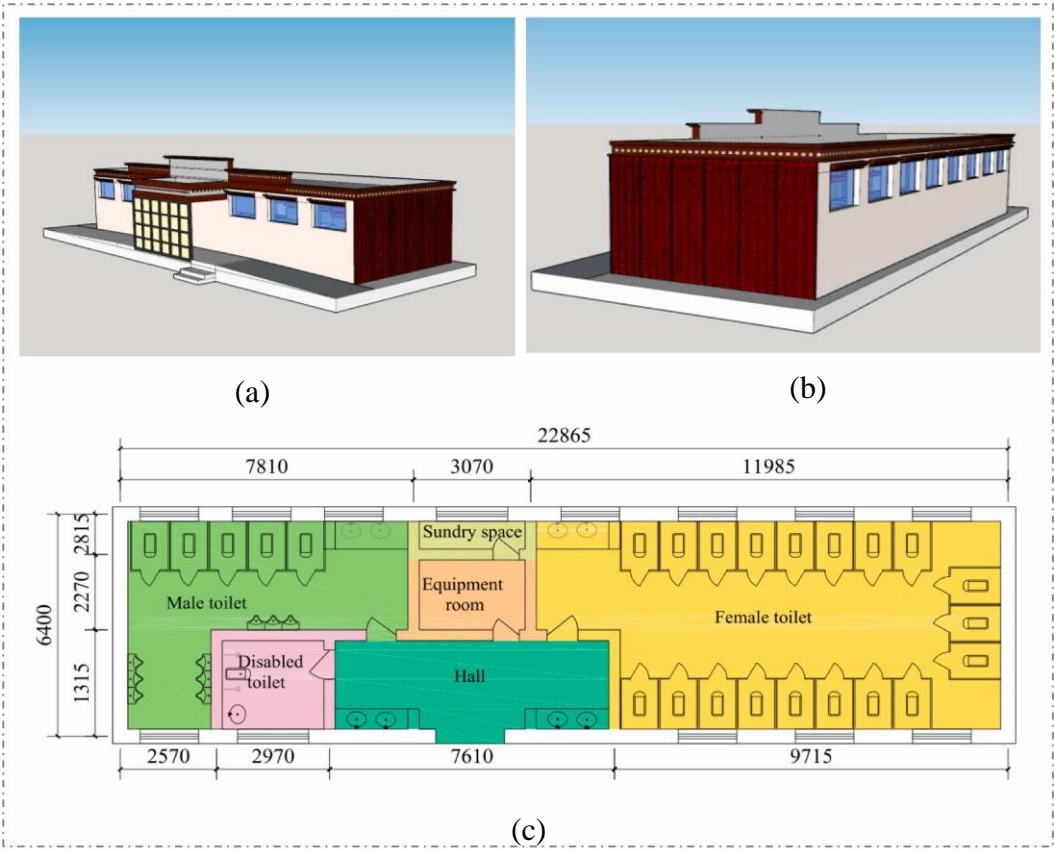


Fig. 6. Public sanitation service building model: (a) North facade, (b) South facade, (c) Building plane.

Table 6
Parameters of building envelope.

Envelope Materials Thickness Heat transfer (mm) coefficient			
(W·m ⁻² ·K ⁻¹)			
External wall	Cement mortar	20	2.39
	Thermal Insulation	25	
	mortar		
	Heavyweight concrete	200	
Interior wall	Cement mortar	20	3.42
	Heavyweight concrete	200	

GPRS communication network. The operation time of the public toilet is from 6:00 to 20:00, and the daily passenger flow is similar throughout the week on any given day (Fig. 8 (e)). The passenger flow reaches the daily peak at ~9:00 and gradually decreases, relatively stable flow until 14:00. The average daily passenger flow is ~1500 people.

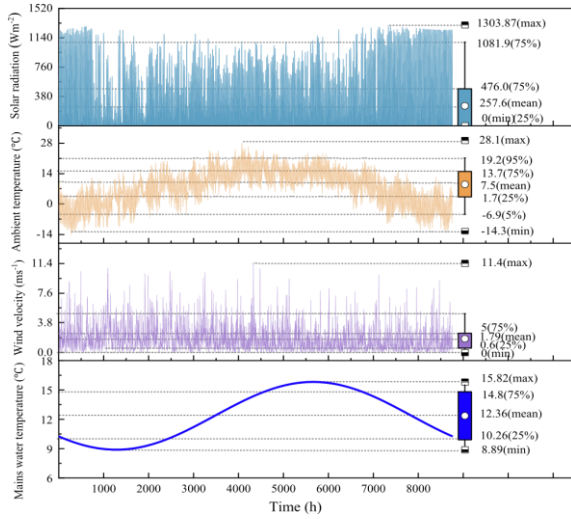


Fig. 7. Ambient temperature, solar radiation intensity and tap water temperature in Lhasa.

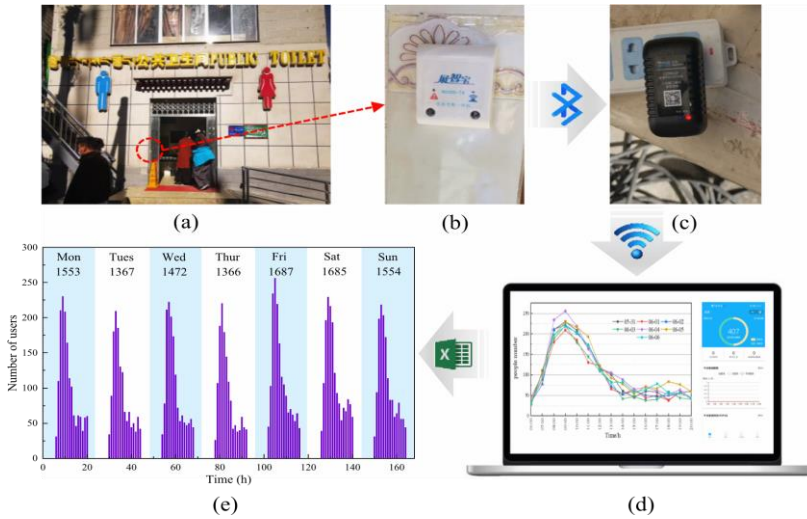


Fig. 8. Visitor flow test and statistics of public toilet in Lhasa: (a) Testing public toilet, (b) Visitor flow counter (c) Signal transmitter, (d) App and computer, (e) Passenger flow data.

Table 7
Power of electrical equipment.

Type	Equipment	Rated power/W	number
Basic Electricity Consumption	Exhaust fan	40	2
	Hand drier	186	2
	Deodorizer	20	7
	Electric lamp	9	11
Heating Electricity Consumption	Air source heat pump	0–15,400	1
	Electric water heater	9000	1
	Circulating fan	800	1
	Heat collecting system water pump	800	1
	Heating system water pump	300	1
	ASHP system water pump	300	1

3.4.4. Building energy load

The building energy load of a PSSB mainly includes space heating load, hot water load, and electrical load. The building energy consumption simulation software Energy Plus simulated the building energy load. To accurately calculate the electrical load, the rated power of each power equipment of the system is given in Table 7, which includes the basic electrical equipment and power and heat source equipment of the heating system.

The hourly heating load, hot water load and electrical load obtained by the simulation are shown in Fig. 9. The annual cumulative heating load is 33545.93 kWh, accounting for 61% of the total load. The annual cumulative hot water load is 17838.99 kWh, accounting for 32% of the total load. The electrical load of basic electrical equipment is 3835.73 kWh, accounting for 7% of the total load.

3.4.5. Equipment price and economic parameters

Table 8 shows the equipment price and economic parameters of SESS. The equipment price is mainly from the existing literature, and the inflation rate and interest rate are from the TRADING ECONOMICS website [53].

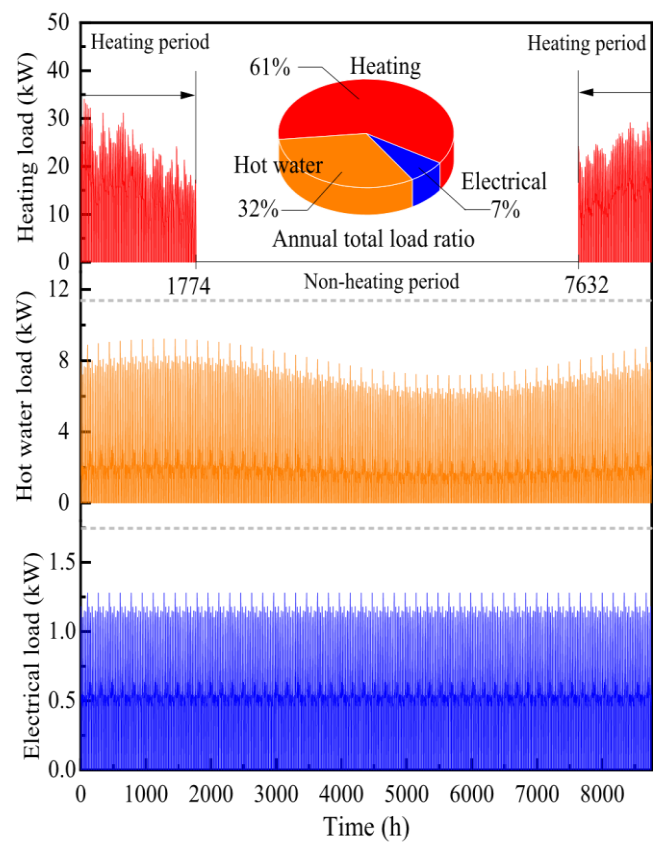


Fig. 9. Heating, hot water and electricity load of the case building.

Table 8
Equipment price and economic parameters of the SESSs.

Parameter	Value [14,31,53]	Unit
Solar collector	500	1500
PV panel	700	CNY·m ⁻²
Battery(200Ah, 12 V)	800	CNY·m ⁻²
Inverter	928	CNY·kW ⁻¹
Air source heat pump		CNY·kW ⁻¹
Electric heater	190	CNY·kW ⁻¹
Heat storage tank	800	CNY·kW ⁻¹
Electricity price	0.74	CNY·m ⁻³
Annual inflation rate	1	CNY·m ⁻³
Annual interest rate	3.85	CNY·kW ⁻¹
		%

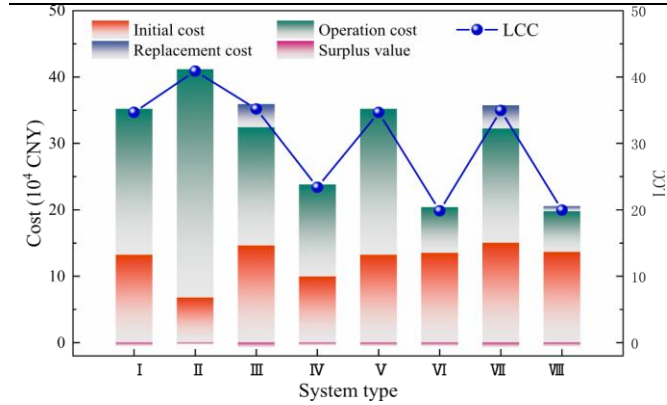


Fig. 10. LCC optimization results of the different solar systems.

Table 9
Optimization results of equipment capacity in different system schemes.

Variables	A_{PV} (m ²)	A_{SC} (m ²)	P_{ASHP} (kW)	C_{Bat} (kWh)	V_{Tank} (m ³)
System I	89.4	—	33.96	—	—
System II	—	30.5	33.93	—	—
System III	88.0	—	33.96	18.96	—
System IV	—	83.9	31.53	—	10.8
System V	89.3	0.1	33.93	—	—
System VI	29.4	87.0	31.26	—	6.9
System VII	93.8	0.1	33.93	18.96	—
System VIII	20.1	96.1	31.26	4.1	7.0

Note: for System II, V and VII, A_{SC} refers to the area of the solar hot air collector, while for System IV, VI and VIII, A_{SC} refers to the area of the solar hot water collector.

4. Results and discussion

The LCC and its composition optimization results for different systems are shown in Fig. 10. The LCC of System VI is the lowest among all system schemes, $\sim 19.85 \times 10^4$ CNY (equivalent to 31,162 USD or 27,535 EURO based on the exchange rate of 12 December 2021). System II has the largest LCC at $\sim 40.89 \times 10^4$ CNY (equivalent to 64,192 USD or 56,722 EURO), about twice that of System VI. The LCC of System I is $\sim 15\%$ lower than that of System II. After adding batteries to the PV system, the LCC of System III is equivalent to that of System I. Although the storage battery reduces the operation cost of the system by storing and regulating the photovoltaic power generation, it also increases the initial investment of the system and adds the replacement cost of the battery.

The LCC of System IV is significantly reduced when adding a heat storage tank in the PT system, which is about 43% lower than that of System II, indicating that the heat storage device plays a crucial role in the PT system with an unstable heat supply. The main reason for this result can be traced back to the energy load characteristics of PSSBs. As shown in Fig. 9, the heating and hot water loads account for more than 90% of the energy consumption, while

the basic power load accounts for only 7%. Overall, the heat load accounts for the vast majority of the system load. System IV can provide electricity for both heating and hot water loads, effectively reducing the energy consumption and cost of the system. The optimized LCC of System V and system VII are similar to those of System I and System III, respectively, indicating that the integration effect of PV and solar hot air collection systems is not significant for PSSBs. The LCCs of System VI and System VIII are $\sim 15\%$ lower than System IV, indicating that the integration gain effect of PV and solar hot water collection systems is more evident than others.

The equipment capacity parameters corresponding to the LCC optimization results of each system are shown in Table 9. The results show that regardless of the type of SESS, the optimal value of solar equipment capacity is greater than the minimum constraint value, which indirectly shows that the application of SESS in PSSBs in Lhasa can reduce the economic cost of the energy supply system to a certain extent. However, there are apparent differences in the equipment capacity configuration of different system schemes. The optimized PV area of the single PV system is much greater than that of a single solar hot air heat collection system. In addition, when the PV system is integrated with a solar hot air heat collection system, the optimized area of the solar collector is close to the lower limit of the constraint, indicating that the integration effect of the two is poor. When the PV system is integrated with the hot water heat storage system, the PV area still accounts for 17% – 25% although the collector area accounts for a large proportion of the system. Moreover, the integration of PV and hot water heat storage system dramatically reduces the operation cost of the system. Although it leads to an increase in the initial investment cost, the LCC of the system is still reduced overall. Therefore, the PV and solar hot water heat integrated collection system with a heat storage tank have more application potential.

4.1. System performance analysis

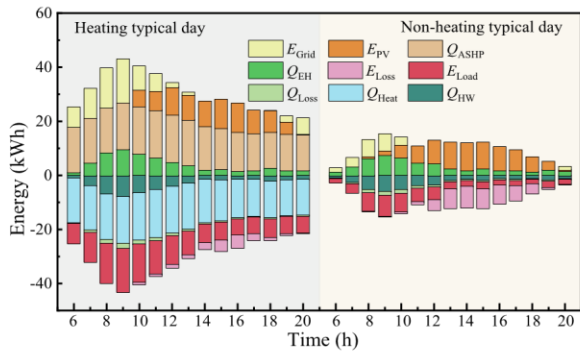
Based on the equipment capacity optimization parameters of the above systems, the operation data of each system under the condition of optimal capacity configuration were obtained through dynamic simulation calculation. The operation performance of each system was analyzed through the data.

4.1.1. Typical daily system performance

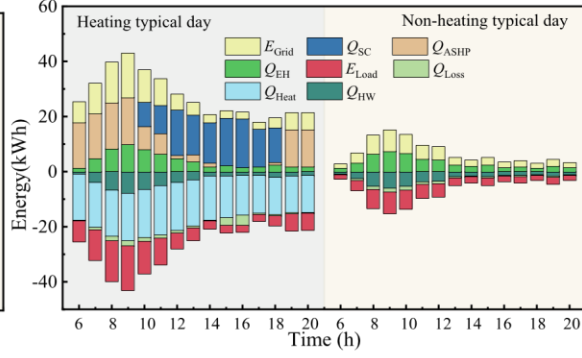
The system operation energy data of a typical heating day and non-typical heating day were selected for analysis from each system's annual operation simulation data to analyze the dynamic operation performance of each system. The energy supplied by the system is a positive value, and the energy consumed or lost by PSSBs is a negative value. The specific operation of each system is shown in Fig. 11.

The dynamic operation of System I is shown in Fig. 11 (a). All the system's energy comes from the PV or the municipal power grid. Electric-driven ASHP and EH supply the heating and hot water loads. During sunny weather, the power required by the system can be fully supplied by the PV system for about 6–7 h during the daytime under heating conditions. In non-heating conditions, the PV system supplies the building load most of the time. Concurrently, the massive difference in the load between heating and non-heating conditions leads to an imbalance between PV power generation and energy demand under non-heating conditions. This leads to numerous episodes of PV power generation loss, with the typical daily power loss reaching 45.58 kWh.

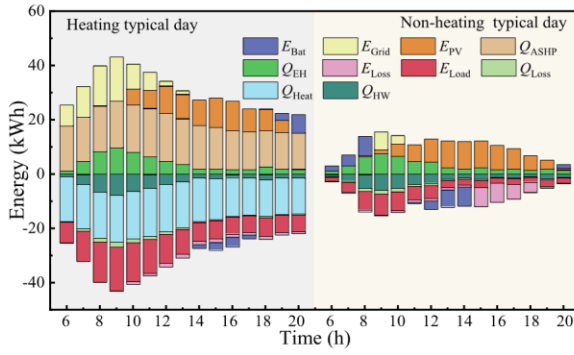
The dynamic operation of System II is shown in Fig. 11 (b). Under typical heating conditions, the heating period of the solar hot air collection system is 10:00 to 18:00, accounting for about 50% of the heating energy consumption. Under non-heating conditions, the municipal power grid bears the entire building load, and the solar heat collection system is idle. Overall, the energy contribution rate of the solar hot air heating system is low.



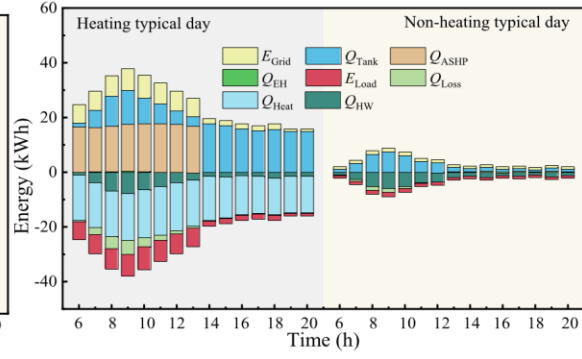
(a) System I



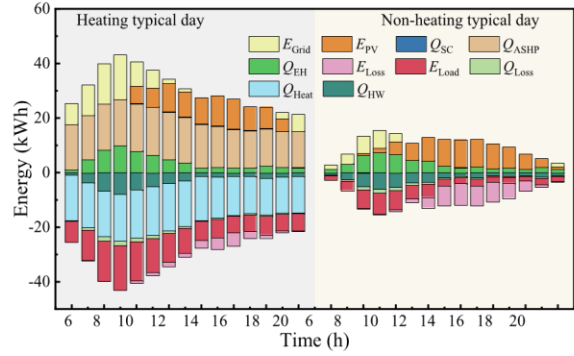
(b) System II



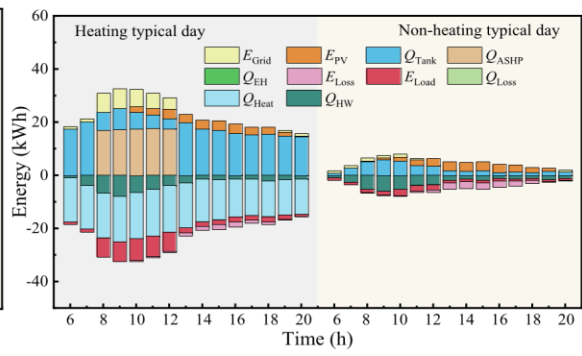
(c) System III



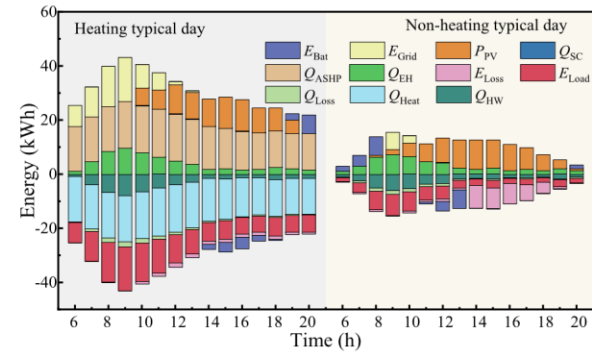
(d) System IV



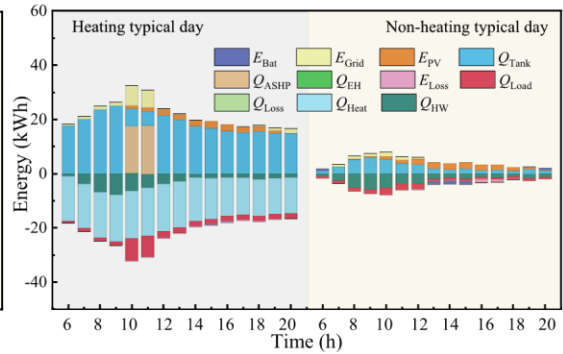
(e) System V



(f) System VI



(g) System VII



(h) System VIII

Fig. 11. The variation of typical daily energy under different solar systems.

Table 10

The annual operation performance of different solar systems.

System type	Electricity		Heat	
	Electricity supply /kWh	Proportion of Electricity consumption	Heat supply and proportion /GJ	
Contrast system:	E_{Grid} : 35033.11		Q_{ASHP} : 120.76 Q_{EH} : 64.22	
System I:	E_{PVt} : 27384.87 E_{PVe} : 15289.75 E_{Grid} : 19743.35		Q_{ASHP} : 120.76 Q_{EH} : 64.22	
System II:	E_{Grid} : 31625.68		Q_{SCt} : 53.03 Q_{SCe} : 45.10 Q_{ASHP} : 75.66 Q_{EH} : 64.22	
System III:	E_{PVt} : 26956.03 E_{PVe} : 18772.66 E_{Grid} : 16260.53		Q_{ASHP} : 120.76 Q_{EH} : 64.22	
System IV:	E_{Grid} : 12834.68		Q_{SCt} : 166.17 Q_{SCe} : 146.15 Q_{ASHP} : 52.11 Q_{EH} : 0.88	
System V:	E_{PVt} : 27354.24 E_{PVe} : 13801.94 E_{Grid} : 19743.98		Q_{SCt} : 0.22 Q_{SCe} : 0.22 Q_{ASHP} : 120.54 Q_{EH} : 64.22	
System VI:	E_{PVt} : 9005.76 E_{PVe} : 4802.84 E_{Grid} : 5969.91		Q_{SCt} : 169.78 Q_{SCe} : 149.22 Q_{ASHP} : 34.91 Q_{EH} : 0.85	
System VII:	E_{PVt} : 28732.67 E_{PVe} : 17909.76 E_{Grid} : 15636.16		Q_{SCt} : 0.22 Q_{SCe} : 0.22 Q_{ASHP} : 120.54 Q_{EH} : 64.22	
System VIII:	E_{PVt} : 6157.00 E_{PVe} : 4738.60 E_{Grid} : 5265.41		Q_{SCt} : 177.49 Q_{SCe} : 149.63 Q_{ASHP} : 26.74 Q_{EH} : 0.68	

Note: E_{PVt} is total power generation of PV system, E_{PVe} is effective power supply of PV power generation, Q_{SCt} is total heat collection of solar collector system, Q_{SCe} is effective heat supply of solar heat collection.

The dynamic operation of System III is shown in Fig. 11 (c). System III is the addition of a battery to System I. The initially lost power of the system is stored in the battery on a typical heating day, and the electricity supply of the power grid is reduced by battery discharge when the PV power supply is insufficient. However, the battery only stores part of the power, and more than half of the PV power generation is lost from operating during typical non-heating days. The PV power generation is greater than the power demand most of the time under non-heating conditions, and the storage and regulation function of the battery is not significant. At the same time, due to the battery's high cost and short service life, the optimized battery capacity is small, which forms the above situation.

The dynamic operation of System IV is shown in Fig. 11 (d). The operation mode of System IV is different from the previous systems. The effective working time of the SESS is effectively prolonged due to the storage and regulation of the heat storage tank. Under typical heating and non-heating conditions, the solar hot water heat storage system continuously provides energy through the end of the day and effectively shortens the working hours of the ASHP and EH. The power supply intensity and total power consumption of the municipal power grid are also reduced.

The dynamic operation of System V is shown in Fig. 11 (e). According to the analysis in Section 5.1, it cannot achieve a good gain effect when the PV system is integrated with the solar hot air heating system. The dynamic

operation conditions of System V and System I on typical days are very similar, which also confirms the above results.

The dynamic operation of System VI is shown in Fig. 11 (f). System VI integrates the PV and solar hot water heat storage systems. On typical days, the energy supply proportion of solar hot water heat storage system is further improved in System VI. The working hours of the ASHP on typical heating days are shortened to 5 h. Part of the power consumption of ASHP is supplied by municipal power and the rest is supplied by the PV system. During non-heating typical days, System VI can operate almost independently of municipal power, but the loss of PV power abandonment is still apparent.

The dynamic operation of System VII is shown in Fig. 11 (g). System VII integrates the solar hot air collector system with System III. However, due to the poor integration effect of the PV system and solar hot air heat collection system, the optimized solar air collector area can be ignored. Therefore, the operation results of System VII and System III are almost the same on a typical day.

The dynamic operation of System VIII is shown in Fig. 11 (h). The solar PV and its power storage system with a solar hot water collector and its heat storage system are integrated into System VIII. From the dynamic operation process of the typical day that the solar hot water heat storage system undertakes most of a PSSBs' thermal load. The heating hours of ASHP on a typical day are further shortened to 2 h, and the municipal power supply is minimized. At the same time, because of

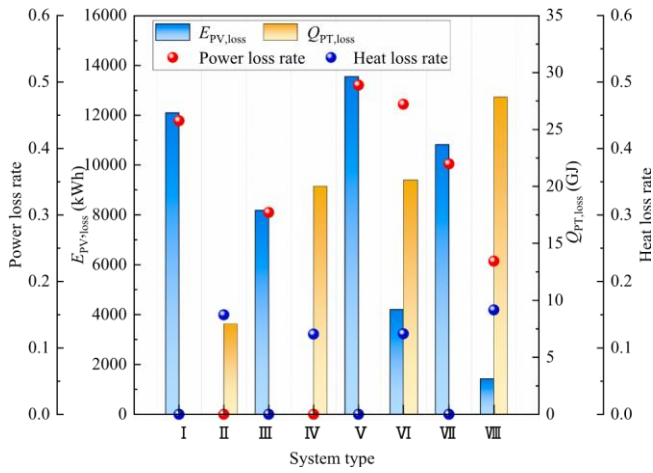


Fig. 12. Annual loss of power generation and heat collection of different solar systems.

the battery, the excess PV power generation is transferred and utilized during the non-heating typical days, which effectively reduces power loss.

4.1.2. Annual system performance

The overall operating performance of each system throughout the year was analyzed based on the analysis of the typical daily dynamic operation performance of the system. Table 10 shows each system's power and heat supply and consumption under annual operating conditions. For a standalone PV system, the total annual power generation of a PV system is 27384.87 kWh, of which ~55.8% of the power. The effective power supply of PV accounts for 43.6% of the total power supply. Because the energy for the heating and hot water loads is supplied by the PV and grid, the power consumption of ASHP and electric water heater accounts for 87.5% of the total power consumption.

For System II, the solar hot air system only undertakes part of the heating load, and thermal energy supplied by the SHS accounts for about 27.5% of the total heating load. The overall conventional power consumption of System II is high throughout the year. Due to the addition of a battery in System III, the effective utilization rate of the PV power generation in the system is increased to 70%, and the effective power supply of the PV system accounts for about 53.6% of the total power supply, which increases by 10% compared to System I.

In System IV, the effective heating capacity of the solar collector system accounts for 73.4% of the total heating capacity, which significantly reduces the consumption of municipal power by ASHP and the electric water heater. Due to the low integration of solar PV and solar hot air system in System V and System VII, the contribution rate of the heat supply of the solar hot air collection system accounts for only 0.1%. Overall, the energy supply structures of System V and System VII are the same as System I.

The solar PV and hot water systems are integrated into System VI and System VIII; more than 80% of the thermal load is provided by the solar hot water system. At the same time, the part of the power load also is provided by the PV system, minimizing the dependence of the system on the municipal grid. In addition to the regulation of solar heat collection by the heat storage tank, the battery also regulates the usage of the system, especially in System VIII. The heat storage tank and storage battery ensure the efficient utilization of PV power generation and heat collection and reduce the overall municipal power need.

The annual loss of power and heat collection of different solar systems are shown in Fig. 12. The PV power generation loss of independent photovoltaic systems and photovoltaic and solar hot air integrated systems is significant. The main reason is that most of the building energy consumption is provided by the PV system, and the scale of the PV cells

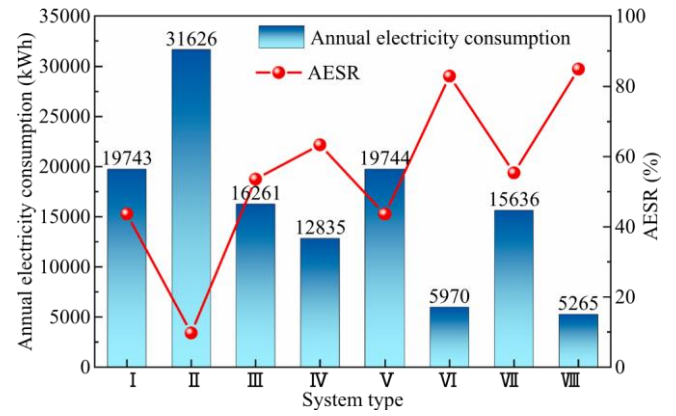


Fig. 13. The E_{ST} and ESR for different SESSs of PSSB.

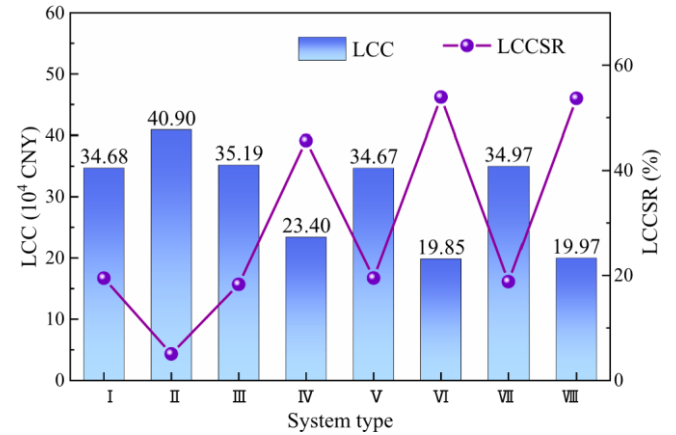


Fig. 14. The LCC and LCCSR for different SESSs.

is large, so it produces more excess power than other systems. In addition, adding batteries to the system can effectively reduce the power loss rate. Compared with the independent PV system, the power loss rate of the PV system with integrated batteries is significantly reduced, from 44% to 30%.

The PV-PT-TES-EES integrated system has the greatest heat loss. Most of the heat load in this system is provided by the solar heat collection system, and the solar collector area is large, producing more excess heat. At the same time, compared with the solar hot air system, the heat loss rate of the solar hot water system integrated heat storage tank is reduced from 15% to 12%.

4.2. Performance comprehensive assessment

Here, the proposed three evaluation indexes of AESR, LCCSR, and ACRR are used to comprehensively evaluate and compare the proposed eight solar energy systems' performance in energy conservation, economy, and environmental protection.

4.2.1. Energy conservation analysis

Fig. 13 shows the annual cumulative conventional power consumption and the annual energy saving ratio of different SESSs in PSSBs. System II consumes the most municipal power, ~31626 kWh per year, with an AESR of only 9.7%. The annually cumulative municipal power consumption of System VIII is the least, ~5265 kWh. The electricity consumption is reduced by about 83.3%, and the AESR increases to 85.0% compared to System II. In addition, the AESR of the single PV system or the PV and solar air heat collection integration system is ~43.6%. When a battery is added to the system, the AESR of System III

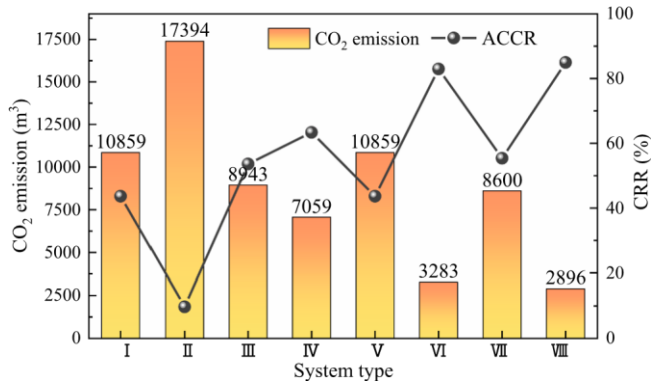


Fig. 15. The annual CO₂ emissions and ACRR for different SESSs.

increases to ~55%, showing that the battery plays a vital role in the energy saving of the single PV system. The AESR of the solar hot water heat collection and storage system is high, 63.4%. When the solar hot water heat storage system is further integrated with the PV system, the AESR of the system significantly improves, reaching 85%.

4.2.2. Economical analysis

The LCC and LCCSR of different SESSs in PSSBs are shown in Fig. 14. LCC and LCCSR trends are similar to the changes in conventional power consumption and AESR of each system. For example, the lowest LCCSR of the system is still System II, which is only 5.05%. The LCCSR of the single PV system and PV and solar hot air integration system is less than 20%. The LCCSR of the solar hot water system and PV and solar hot water integration system is high, reaching ~50%.

Different from the AESR, the LCCSR of System VI is the greatest. Although the operation cost of System VIII is low, the equipment cost and replacement cost are much greater than that of System VI. Therefore, the economy of System VI is slightly better than that of System VIII when accounting for the whole life cycle of the system.

4.2.3. CO₂ reduction analysis

The annual CO₂ emissions and ACRR of the different SESSs in PSSBs are shown in Fig. 15. Due to the lack of carbon emission data during the SESS equipment production, manufacturing, and abandonment, only the carbon emissions during the system operation stage are considered in the environmental evaluation. The carbon emission in the operation stage is directly related to a system's power consumption.

The annual CO₂ emission of the contrast system reaches 19262.5 m³. The annual CO₂ emission of System II is the greatest, and System VIII is the least. There are different degrees of differences in equipment types and specifications in each system, leading to specific differences in the carbon emissions of equipment in each system. Therefore, the carbon emission of the equipment itself in the life cycle will be considered in future work on the environmental benefit evaluation of the SESS once

the basic carbon emission data of the equipment are available. Such evaluation results will be more objective and practical.

The performance parameters of each system's energy conservation, economic and CO₂ emission reduction are summarized in Table 11. The coloring of the cells in the table indicates good or bad performance, with warmer colors indicating better system performance and colder colors indicating worse system performance. System VIII has the best energy conservation and carbon emission reduction capacity, and its economy is second only to System VI across all systems. The LCCSR difference between these two systems is minimal, less than 1%. The above research results show that different SESSs have different advantages in economy, energy conservation, and environmental protection compared with the traditional electric energy system for PSSBs in Lhasa. Overall, the integrated system of PV-PT-TES-EES has the best comprehensive performance.

4.3. Sensitivity analysis

To understand the influence of non-variable parameters on the optimization results of a SESS, the sensitivity analysis of system optimization results to non-variable parameters was performed. The sensitivity analysis is divided into two parts according to the type of parameters: first, sensitivity analysis of electricity price, annual inflation rate, and annual interest rate; second, sensitivity analysis of the unit cost of equipment, such as collector, water tank, PV module, battery, and ASHP. Because System VIII has numerous advantages in many areas, it is used as an example for sensitivity analysis.

4.3.1. Economic parameters

The economic parameters of electricity price, inflation rate, and

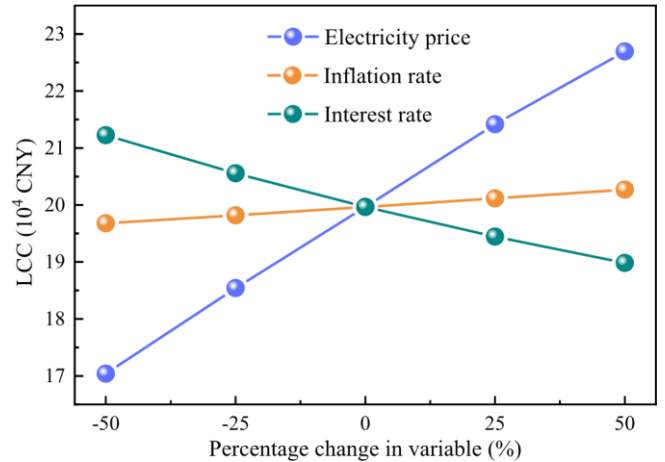
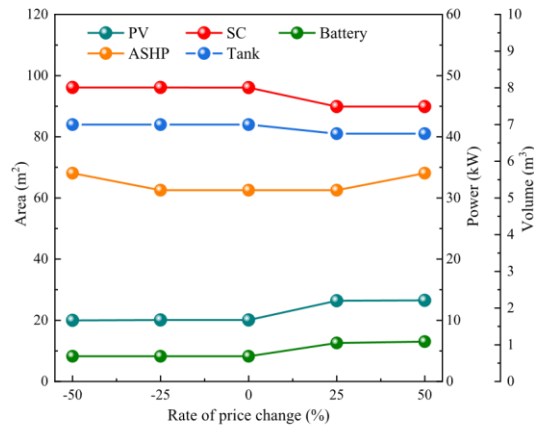


Fig. 16. Effects of electricity price, interest rate and inflation rate on system life cycle cost.

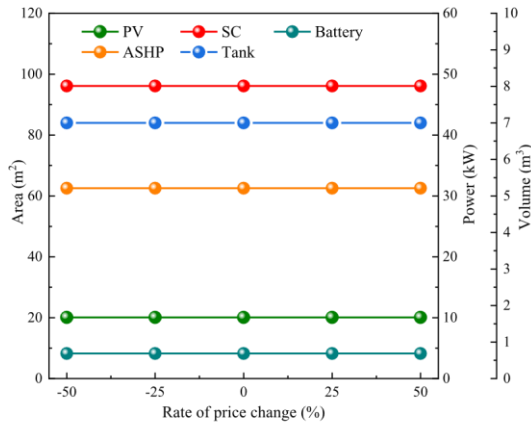
Table 11

The results of system assessment of different solar systems.

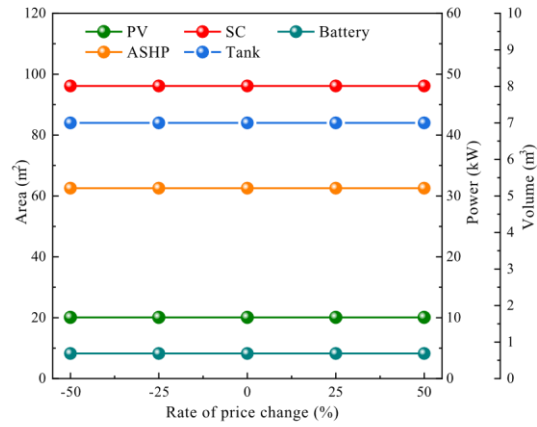
System type	Energy saving		Economy		CO ₂ emission reduction	
	<i>E_{ss}</i> (kWh)	<i>AESR</i> (%)	<i>LCC_{ST}</i> (CNY)	<i>LCCSR</i> (%)	<i>L_{CO2}</i> (m ³)	<i>ACRR</i> (%)
System I	19743.35	43.64	34.68×10 ⁴	19.49	10858.84	43.64
System II	31625.68	9.73	40.90×10 ⁴	5.05	17394.12	9.73
System III	16260.53	53.59	35.19×10 ⁴	18.31	8943.29	53.59
System IV	12834.68	63.36	23.40×10 ⁴	45.67	7059.07	63.36
System V	19743.98	43.64	34.67×10 ⁴	19.50	10859.19	43.64
System VI	5969.91	82.96	19.85×10 ⁴	53.91	3283.45	82.95
System VII	15636.15	55.37	34.97×10 ⁴	18.81	8599.88	55.35
System VIII	5265.41	84.97	19.97×10 ⁴	53.65	2895.97	84.97



(a) electricity price



(b) inflation rate



(c) interest rate

Fig. 17. Effects of electricity price, interest rate and inflation rate on optimized capacity of equipment.

interest rate decreased by 25% and 50%, and increased by 25% and 50%, respectively, based on the existing values. The new economic parameter value was used for the optimization simulation. The sensitivity analysis results of electricity price, inflation rate, and interest rate on the LCC of System VIII are shown in Fig. 16. The LCC increases with the increase in electricity price and inflation rate and decreases with an increase in the interest rate. The variation rate of LCC with a change in electricity price is the greatest, followed by the annual interest rate, and the lowest, the inflation rate. The electricity price

increased from 0.37 CNY·kWh⁻¹ to 1.11 CNY·kWh⁻¹, and the LCC of System VIII increased by 11.8%. According to the energy performance analysis of the above systems throughout the year, the annual conventional power consumption of System VIII is the lowest. Therefore, the impact of electricity price on the LCC is more significant for other systems.

The effects of electricity price, interest rate, and inflation rate on the optimized equipment capacity are shown in Fig. 17. The variation in

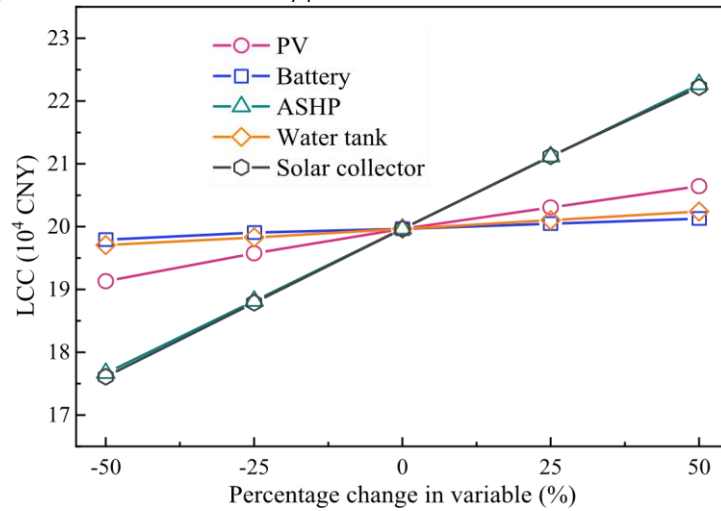


Fig. 18. Effects of equipment price on system life cycle cost.

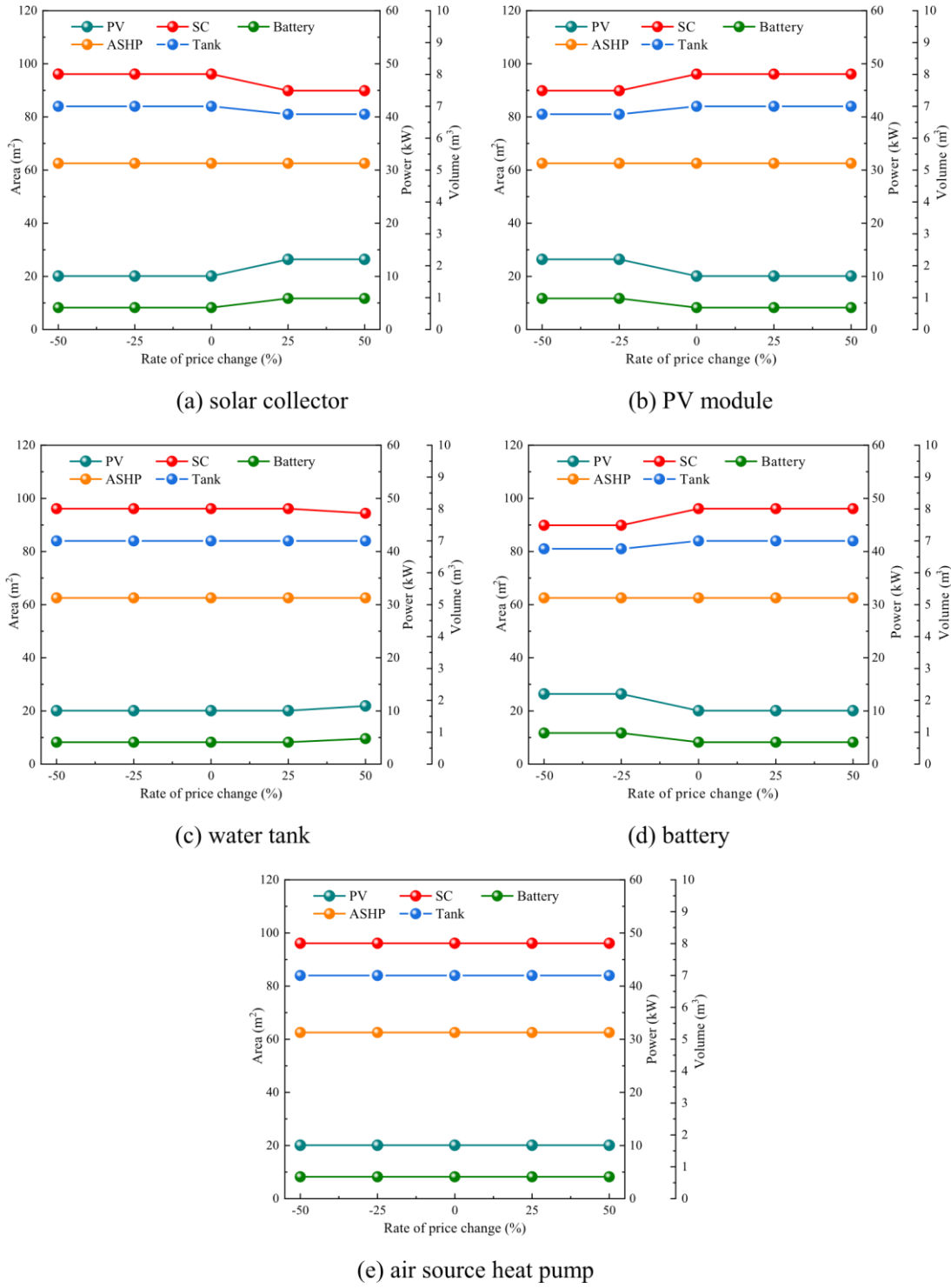


Fig. 19. Effects of equipment price on optimized capacity of equipment.

electricity price significantly impacts the optimized capacity of each piece of equipment, while the variation in the interest rate and inflation rate does not cause the change in optimized capacity. The optimized photovoltaic area and battery power show an increasing trend with the increase in electricity price, which indicates that with the increasing price of municipal power, photovoltaic power becomes more competitive. The optimized solar collector area and water tank value show a decreasing trend with increasing electricity prices. Because the total area of PV and PT equipment that can be laid on a roof is limited, an increase in system LCC caused by an increase in the number of

photovoltaic modules is lower than that caused by an increase in the collector area. Therefore, an increase in the photovoltaic area leads to a decrease in the collector area. The air source heat pump's optimized power decreases first and then increases with an electricity price increase because it is economical to use the higher power ASHP to consume electricity for heating when the electricity price is low. When the electricity price is high, the PV power supply increases and the heat supply of the collector decreases. It is also necessary to increase the power of the ASHP to supply more heat.

4.3.2. Equipment price

The sensitivity analysis results of System VIII equipment price to its LCC are shown in Fig. 18. The equipment price of System VIII decreases by 25% and 50%, and increases by 25% and 50%, respectively, based on the existing values. The LCC increases with an increase in the price of the solar collector, PV module, heat storage tank, battery, and ASHP. The degree of influence of equipment price on LCC from large to small is: solar collector/ASHP > PV module > heat storage tank > battery. Although the price per unit area of a collector is low, the optimized collector area is large, so the change in collector price significantly impacts the LCC of the system. The price change of an ASHP will also significantly impact the LCC due to the high cost per unit of thermal power. In comparison, the optimized PV cost is greater than that of a battery and heat storage tank, so the system LCC is more sensitive to a change in the price of PV.

The effects of equipment price on the optimized equipment capacity are shown in Fig. 19. From Fig. 19 (a), the optimized collector area and water tank volume decrease, and the photovoltaic area and battery power increase with an increase in the collector price. From Fig. 19 (b) and 19 (d), the optimized PV area and battery power increase, and collector area and water tank volume decrease with a PV module and battery price increase. From Fig. 19 (c), the optimized PV area and battery power increase slightly, the collector area decreases, and the water tank volume and the power of ASHP remain unchanged with an increase in water tank price. From Fig. 19 (e), the optimal capacity of each piece of equipment remains unchanged with an increase in the price of the air source heat pump.

5. Conclusions

The optimization model of eight potential SESS for PSSBs was established, and the equipment capacity in each system was optimized, respectively. Furthermore, the short-term dynamic operation performance and the energy conservation, economic and CO₂ emission reduction performance of the systems were comprehensively analyzed. The specific conclusions are as follows:

(1) For PSSBs, the optimized LCC of a single solar hot air system is the maximum. Compared with a single solar hot air system, the optimized LCC of a single photovoltaic system is reduced by 15%, and that of a solar hot water and heat storage integrated system is reduced by about 43%.

(2) Compared with the traditional municipal power supply system, a SESS has significant energy savings, economics, and environmental protection benefits. Overall, the optimized integrated System VIII has the best comprehensive performance. The AESR of the system is 85%, the LCCSR is 50%.

(3) The electricity price is the most significant factor for LCC compared to the annual interest and inflation rates. The price of a solar collector and ASHP have the most significant impact on the LCC optimization results of a PV-PT system with battery and thermal storage.

There are several limitations of this study. Firstly, the minimum life cycle cost was taken as the optimization goal to analyze the suitability of different solar systems in PSSBs. For scenarios with high-reliability requirements for energy conservation and carbon emission reduction rates, multi-objective optimization methods should be adopted to coordinate the contradiction between different objectives to obtain more balanced system optimization design results. Secondly, considering the current grid connection of PV power in Lhasa, Tibet, the excess power of the PV system was not added to the national grid in this study. If the grid conditions permit, the two-way of PV will positively reduce excess power loss. Therefore, the effect of grid connection of excess PV power on the optimization results should be analyzed in future research. Despite the limitations, the conclusions of this paper are still valuable for the scheme determination and optimization design of solar energy supply systems for PSSBs in solar energy resource-rich areas.

CRedit authorship contribution statement

Yaowen Chen: Conceptualization, Resources, Writing – review & editing.
Mengchen Quan: Conceptualization, Methodology, Writing – review & editing.
Dengjia Wang: Conceptualization, Supervision, Writing – review & editing. **Hu Du:** Conceptualization, Supervision, Writing – review & editing. **Liang Hu:**

Methodology, Writing – review & editing. **Yiting Zhao:** Methodology, Writing – review & editing. **Mengmeng Guo:** Writing – review & editing. **Yanfeng Liu:** Conceptualization, Writing – review & editing.

Declaration of Competing Interest

The authors declare that they have no known competing financial interests or personal relationships that could have appeared to influence the work reported in this paper.

Acknowledgements

This study was supported by National Key R&D Program of China (No. 2021YFE0113500), National Natural Science Foundation of China (No. 52108094, 51878532), the State Key Program of National Natural Science Foundation of China (No. U20A20311), Key laboratory scientific research program of Shaanxi Provincial Department of Education (No. 21JS029), Cardiff University Global Challenge Research Fund and the British Council Researcher Links Grant (No. 2017-RLWK9-10863).

Appendix A. Supplementary data

Supplementary data to this article can be found online at <https://doi.org/10.1016/j.enconman.2022.115847>.

References

- [1] Chu X. Study on the eco-environmental effects of tourism development on the Qinghai-Tibet plateau. Zhejiang Normal University, 2020. (In Chinese).
- [2] He Y, Li J. "The Toilet Revolution" in the cities of Tibet since the mid of twentieth century. J. Tibet Univ. 2019;3:168–74. In Chinese.
- [3] Fang Y, Wei Y. Climate change adaptation on the Qinghai-Tibetan Plateau: the importance of solar energy utilization for rural household. Renew Sustain Energy Rev 2013;18:508–18.
- [4] Liu W, Lund H, Mathiesen BV, Zhang X. Potential of renewable energy systems in China. Appl Energy 2011;88(2):518–25.
- [5] Sayigh AAM, editor. Solar energy application in buildings. New York: Academic Press; 1979.
- [6] Kreith F. Solar heating and cooling: active and passive design. CRC Press; 1982.
- [7] Kulkarni GN, Kedare SB, Bandyopadhyay S. Determination of design space and optimization of solar water heating systems. Sol Energy 2007;81(8):958–68.
- [8] Zhang R, Wang D, Liu Y, Chen Y, Fan J, Song C, et al. Economic optimization of auxiliary heat source for centralized solar district heating system in Tibetan Plateau. China Energy Convers. Manage. 2021;243:114385.
- [9] Wang D, Mo Z, Liu Y, Ren Y, Fan J. Thermal performance analysis of large-scale flat plate solar collectors and regional applicability in China. Energy 2022;238:121931.
- [10] Xu G, Zhao S, Zhang X, Zhou X. Experimental thermal evaluation of a novel solar collector using magnetic nano-particles. Energy Convers Manage 2016;130:252–9.
- [11] Saxena A, Srivastava G, Tirth V. Design and thermal performance evaluation of a novel solar air heater. Renewable Energy 2015;77:501–11.
- [12] Palacio M, Rincon A, Carmona M. Experimental comparative analysis of a flat plate solar collector with and without PCM. Sol Energy 2020;206:708–21.
- [13] Pandey AK, Tyagi VV, Rahim NA, Kaushik SC, Tyagi SK. Thermal performance evaluation of direct flow solar water heating system using exergetic approach. J Therm Anal Calorim 2015;121(3):1365–73.
- [14] Huang J, Fan J, Furbo S, Chen D, Dai Y, Kong W. Economic analysis and optimization of household solar heating technologies and systems. Sustainable Energy Technol Assess 2019;36:100532.
- [15] Martinopoulos G, Tsalikis G. Active solar heating systems for energy efficient buildings in Greece: a technical economic and environmental evaluation. Energy Build 2014;68:130–7.
- [16] Hobbi A, Siddiqui K. Optimal design of a forced circulation solar water heating system for a residential unit in cold climate using TRNSYS. Sol Energy 2009;83(5): 700–14.
- [17] Ko MJ. Analysis and optimization design of a solar water heating system based on life cycle cost using a genetic algorithm. Energies 2015;8(10):11380–403.
- [18] Qiu G, Yu S, Cai W. A novel heating strategy and its optimization of a solar heating system for a commercial building in term of economy. Energy 2021;221:119773.
- [19] Villasmil W, Troxler M, Hendry R, Schuetz P, Worlitschek J. Control strategies of solar heating systems coupled with seasonal thermal energy storage in self-sufficient buildings. J Storage Mater 2021;42:103069.
- [20] Wang Y, Rao Z, Liu J, Liao S. An optimized control strategy for integrated solar and air-source heat pump water heating system with cascade storage tanks. Energy Build 2020;210:109766.
- [21] Baljit SSS, Chan HY, Sopian K. Review of building integrated applications of photovoltaic and solar thermal systems. J Cleaner Prod 2016;137:677–89.

- [22] Singh D, Rawat M, Singh SP, et al. Performance of PV integrated wall and roof as a building material. *IOP Conf. Series: Mater. Sci. Eng.* IOP Publish. 2021;1033(1): 012005.
- [23] Peng J, Curcija DC, Thanachareonkit A, Lee ES, Goudey H, Selkowitz SE. Study on the overall energy performance of a novel c-Si based semitransparent solar photovoltaic window. *Appl Energy* 2019;242:854–72.
- [24] Sun LL, Yang HX. Impacts of the shading-type building-integrated photovoltaic claddings on electricity generation and cooling load component through shaded windows. *Energy Build* 2010;42(4):455–60.
- [25] Jie Ji, Hua Yi, Wei He, Gang P, Jianping Lu, Bin J. Modeling of a novel Trombe wall with PV cells. *Build Environ* 2007;42(3):1544–52.
- [26] Arslan E, Aktas M, Can OF. Experimental and numerical investigation of a novel photovoltaic thermal (PV/T) collector with the energy and exergy analysis. *J Cleaner Prod* 2020;276:123255.
- [27] Barbu M, Siroux M, Darie G. Numerical model and parametric analysis of a liquid based hybrid photovoltaic thermal (PVT) collector. *Energy Rep* 2021;7:7977–88.
- [28] Wang Y, Ji J, Sun W, Yuan W, Cai J, Guo C, et al. Experiment and simulation study on the optimization of the PV direct-coupled solar water heating system. *Energy* 2016;100:154–66.
- [29] Behzadi A, Arabkoohsar A, Yang Y. Optimization and dynamic techno-economic analysis of a novel PVT-based smart building energy system. *Appl Therm Eng* 2020; 181:115926.
- [30] Herrando M, Pantaleo AM, Wang K, Markides CN. Solar combined cooling, heating and power systems based on hybrid PVT, PV or solar-thermal collectors for building applications. *Renewable Energy* 2019;143:637–47.
- [31] Kavian S, Aghanajafi C, Jafari Mosleh H, Nazari A, Nazari A. Exergy, economic and environmental evaluation of an optimized hybrid photovoltaic-geothermal heat pump system. *Appl Energy* 2020;276:115469.
- [32] Alptekin E, Ezan MA. Performance investigations on a sensible heat thermal energy storage tank with a solar collector under variable climatic conditions. *Appl Therm Eng* 2020;164:114423.
- [33] Zhao J, Ji Y, Yuan Y, Zhang Z, Lu J. Energy-saving analysis of solar heating system with PCM storage tank. *Energies* 2018;11(1):237.
- [34] Ucar A, Inalli M. Thermal and economic comparisons of solar heating systems with seasonal storage used in building heating. *Renewable Energy* 2008;33(12):2532–9.
- [35] Sharma P, Kolhe M, Sharma A. Economic performance assessment of building integrated photovoltaic system with battery energy storage under grid constraints. *Renewable Energy* 2020;145:1901–9.
- [36] Vieira FM, Moura PS, de Almeida AT. Energy storage system for self-consumption of photovoltaic energy in residential zero energy buildings. *Renewable Energy* 2017;103:308–20.
- [37] Gu Y. Power grid quality analysis of grid-connected distributed PV generation system. Jiangsu university, 2018. (In Chinese).
- [38] Zheng R, He T, Lu B, Jiao Q. Technical code for solar heating system (GB50495- 2019). Beijing: China Building Industry Press; 2019. In Chinese.
- [39] D.J. A., B.W. A., *Solar Engineering of Thermal Processes*, John Wiley & Sons, Inc.
- [40] Hassan Q, Jaszczur M, Przenzak E, Suwała W, Dudek M, Leszczynski J, et al. Mathematical model for the power generation from arbitrarily oriented photovoltaic panel. *EDP Sciences* 2017;14:01028.
- [41] Luque A, Hegedus S. *Handbook of photovoltaic science and engineering*. John Wiley & Sons; 2011.
- [42] Hu L, Liu Y, Wang D, Luo Xi, Liu H. Feasibility analysis and feature comparison of cold thermal energy storage for off-grid PV air-conditioned buildings in the tropics. *Energy Convers Manage* 2022;254:115176.
- [43] Jia H, Peng J, Li N, et al. Optimization and economic analysis of distributed photovoltaic-energy storage system under dynamic electricity price. *Acta Energy Solaris Sinica* 2021;42(5):187–93. In Chinese.
- [44] Ozcan HG, Varga S, Gunerhan H, Hepbasli A. Numerical and experimental work to assess dynamic advanced exergy performance of an on-grid solar photovoltaic-air source heat pump-battery system. *Energy Convers Manage* 2021;227:113605.
- [45] Liu Y, Zhou W, Luo Xi, Wang D, Hu X, Hu L. Design and operation optimization of multi-source complementary heating system based on air source heat pump in Tibetan area of Western Sichuan. *China Energy Build* 2021;242:110979.
- [46] Najafi Ashtiani M, Toopshekan A, Razi Astaraei F, Yousefi H, Maleki A. Techno-economic analysis of a grid-connected PV/battery system using the teaching-learning-based optimization algorithm. *Sol Energy* 2020;203:69–82.
- [47] Marszal AJ, Heiselberg P. Life cycle cost analysis of a multi-storey residential Net Zero Energy Building in Denmark. *Energy* 2011;36(9):5600–9.
- [48] Huang LX. Objection to the estimated net residual value of fixed assets. *Finance Account Monthly* 2004;19:30–1. In Chinese.
- [49] Riffonneau Y, Bacha S, Barruel F, et al. Optimal reactive supervision of grid connected PV systems with batteries in real conditions. *Int Rev Electr Eng* 2012;7: 4607–15.
- [50] Zhou Q, Ju Y, Zhou C. An effective inverse analysis of cohesive parameters of flexible adhesive joints based on the Hooke-Jeeves algorithm. *Eng Mech* 2015;32(4):1–7. In Chinese.
- [51] Pan F, Li W, Gao Q. Particle swarm optimizer and multi-object optimization. Beijing: Beijing Institute of Technology Press; 2013.
- [52] Zeng R, Zhang X, Deng Y, Li H, Zhang G. Optimization and performance comparison of combined cooling, heating and power/ground source heat pump/ photovoltaic/solar thermal system under different load ratio for two operation strategies. *Energy Convers Manage* 2020;208:112579.
- [53] TRADING ECONOMICS. (2021). <https://zh.tradingeconomics.com>. (Accessed 25 August 2021).